INFORMATION TO USERS

This manuscript has been reproduced from the microfilm master. UMI films the text directly from the original or copy submitted. Thus, some thesis and dissertation copies are in typewriter face, while others may be from any type of computer printer.

The quality of this reproduction is dependent upon the quality of the copy submitted. Broken or indistinct print, colored or poor quality illustrations and photographs, print bleedthrough, substandard margins, and improper alignment can adversely affect reproduction.

In the unlikely event that the author did not send UMI a complete manuscript and there are missing pages, these will be noted. Also, if unauthorized copyright material had to be removed, a note will indicate the deletion.

Oversize materials (e.g., maps, drawings, charts) are reproduced by sectioning the original, beginning at the upper left-hand corner and continuing from left to right in equal sections with small overlaps. Each original is also photographed in one exposure and is included in reduced form at the back of the book.

Photographs included in the original manuscript have been reproduced xerographically in this copy. Higher quality 6" x 9" black and white photographic prints are available for any photographs or illustrations appearing in this copy for an additional charge. Contact UMI directly to order.

UMI

A Bell & Howell Information Company
300 North Zeeb Road, Ann Arbor MI 48106-1346 USA
313/761-4700 800/521-0600

Université d'Ottawa · University of Ottawa

Polarization Mode Dispersion in Cascaded Optical Fibre Communication Links

by Sacha E. Corbeil

A thesis submitted to the Faculty of

Graduate Studies and Research in partial

fulfillment of the requirements for the degree

of

Master of Applied Science

Department of Electrical Engineering

University of Ottawa
Ottawa, Ontario
Thursday, December 10, 1998

ABSTRACT

Polarization mode dispersion (PMD) in single mode optical fibres refers to the phenomenon present in all real fibres that results in the different polarization components of the signal launched into the fibre to travel at different speeds, producing a different propagation delay for each component. This differential group delay (DGD) represents a source of intersymbol interference for digital communications. It can be of a sufficient magnitude that it becomes a problem in ultra high bit-rate systems, and thus its study, and the development of engineering models to determine its magnitude and impact on system performance are of significant interest.

PMD arises from deviations of a fibre from its ideal uniform shape. These deviations arise from a variety of unpredictable causes, which allows us to treat DGD as a random process of several variables such as wavelength or frequency, time, temperature, etc. Measurements of DGD thus need to be made to characterize this random process, and are not one instance of this phenomenon in a fibre.

In this thesis, the theoretical models describing the physical origins of DGD are presented, and methods of measuring the DGD process are discussed. Three measurement methods are evaluated for their practical usefulness (Jones matrix eigen-analysis, wavelength-scanning and interferometric techniques). Characterization based on measurements of the mean and correlation coefficients of the DGD process with respect to time, wavelength/frequency and temperature are made using the Jones matrix eigen-analysis method. A comparison between the measurements and numerical simulations based on the physical models of the origins of PMD are made. Measurements of the DGD of a system's components and the overall system are made to validate the theoretical models we have that

describe how component DGD relates to the overall system DGD. The results of the measurement agree with the theoretical models that the DGD is described by a Maxwellian distribution, and support the cascaded link rule for predicting the system DGD; the correlation bandwidth measurement is seen to agree with the findings of the numerical simulations.

ACKNOWLEDGEMENTS

My gratitude is extended to Dr. M. O'Sullivan at NORTEL for his supervision of my work. Sincere thanks also go to Dr. P. Galko at University of Ottawa, and Dr. J. Chrostowski at the National Research Council for their valuable comments and suggestions as well as offering laboratory access at NRC. I am also grateful to T. Taraschuk, D. Atkinson, K. Visvanatha and NORTEL for time and use of the laboratory and equipment; and of course, my wife Jessica and my family for their support and encouragement.

Table Of Contents

List Of Figures

List Of Tables

List of Acronyms

BER .....bit-error rate

DCF .....dispersion compensating fibre

DCM .....dispersion compensating module

DGD .....differential group delay

EDFA .....erbium doped fibre amplifier

FWHM.....full-width at half-maximum

JME.....Jones matrix eigen-analysis

LED .....light-emitting diode

NDSF.....non-dispersion-shifted fibre

NRZ .....non-return to zero

OC-48 .....optical carrier-48, data rate of 2.48832 GBit/s

OC-192 .....optical carrier-192, data rate of 9.953280 GBit/s

PDL.....polarization-dependent loss

PMD .....polarization mode dispersion

PMF .....polarization maintaining fibre

PSP .....principal state of polarization

RMS.....root mean square

RSS .....root sum of squares

SMF .....single mode fibre

SOP.....state of polarization

Definition of Symbols

α.....attenuation, p. 31.

$C_\lambda(\Delta\lambda)$ .....normalized DGD autocovariance function with respect to wavelength, p. 28.

$C_{t,\lambda_1}(\Delta t)$ .....normalized DGD autocovariance function with respect to time, at a fixed wavelength, p. 29.

$C_t(t)$ .....normalized DGD autocovariance function with respect to time, averaged over wavelength, p. 30.

c_0.....velocity of light in vacuum, p. 11.

χ_0^2.....goodness-of-fit test parameter, p. 60.

$\Delta\lambda_c$ .....correlation bandwidth expressed as a wavelength separation, p. 28.

$\Delta\omega_c$ .....correlation bandwidth expressed as a frequency separation, p. 29.

$\Delta\tau_i$ .....differential section delay in section *i*, p. 9.

$\Delta\tau(\lambda)$ .....instantaneous DGD as a function of wavelength, p. 28.

$\langle\Delta\tau\rangle$, or $\overline{\Delta\tau}$ .....mean differential group delay, p. 23.

E_x.....electric field component along horizontal axis, p. 13.

$\vec{E}_{\text{in, out}}$ .....Jones vector representing input / output electric field, p. 14.

$e^{\beta(\omega)}$ .....complex propagation exponential, taking into account attenuation and absolute phase, p. 14.

$\varepsilon_{\text{in, out}}$ .....magnitude of electric field, p. 14.

$e^{i\phi_{\text{in, out}}}$ .....complex exponential, taking into account absolute phase of

electric field, p. 14.

$\hat{e}_{in}$ .....normalized Jones vector representing launch state of polarization of electric field, p. 31.

$\hat{\varepsilon}_{in,\ out}$ .....Jones vector, representing electric field, normalized to unity, p. 31.

$\hat{J}$ .....Jones vector describing polarized light, p. 13.

k_{ω}, k_{λ}.....correlation bandwidth constants, p. 29.

L.....fibre length, p. 10.

l.....average mode coupling length, p. 10.

λ .....wavelength, p. 11.

$n_{\chi}(\lambda)$ .....refractive index along horizontal axis at given wavelength, p. 11.

$j\Psi(\omega)$ .....complex phase factor, p. 31.

$<P>$ .....mean penalty due to PMD, measured as eye-closure and given in dB, p. 36.

R.....transposed polarization transmission Jones matrix relating the differential delay matrices of two concatenated fibres, p. 20.

$\rho_{1/2}$.....eigenvalues of Jones matrix DGD measurement technique eigen-equation, p. 40.

$\hat{s}$ .....unitary Stokes vector representing polarized light, p. 10.

$s_{1/2/3}$ .....Stokes parameters, coefficients of the Stokes vector, p. 15.

T.....Jones transmission matrix, p. 13.

T_b .....bit period, p. 33.

θ_i .....angle between slow linear axis and horizontal axis, p. 9.

$\theta_{1\text{-}2}$.....angle between Stokes output PSP of first fibre and Stokes input PSP into second fibre, p. 20.

$U(\omega)$.....unitary Jones matrix, p. 14.

$u_{1/2}(\omega)$.....unitary Jones matrix coefficients, p. 14.

Chapter 1: Introduction

The demand for data communications is increasing at an unprecedented rate due to such applications as the Internet, business transactions being conducted electronically, and tele-commuting. The volume of data communications has recently surpassed that of voice communications in many telephone networks. The demand is driven by technology, and must be satisfied by technology. In order to sustain such future data traffic flows, present networks must improve switching and increase transmission capacity.

Fibre optic technology provides high speed telecommunications and is key to supplying future needs for transport capacity. While optical fibres have tremendously large bandwidths and low noise, and consequently large transmission capacity, various difficulties have limited the bit-rates which can be achieved in practice. Techniques have been developed in the recent past to deal with obstacles associated with increasing the speed of optical communication links. For example, modal dispersion caused by light travelling along many paths in a multi-mode fibre was removed by creating single mode fibre: a fibre whose core is only large enough to allow one optical wave mode to travel through it. Chromatic dispersion, which results from varying indices of refraction with optical frequency causing distortion in digital signals, has been dealt with by inserting dispersion compensators throughout an optical communications link which compensate for the variation in index of refraction responsible for chromatic dispersion.

With multi-mode and chromatic dispersion compensated, digital signalling at the OC-48 rate (approximately 2.5 GBit/s) can be achieved in practice. To increase capacity in an optical fibre, wavelength and time division multiplexing (WDM and TDM) are the key methods. WDM consists of modulating multiple signals onto optical channels of separate

wavelengths, and transmitting them along the same fibre. TDM consists of reducing the bit period and interleaving multiple signals together in a single channel, thereby increasing the bit-rate. In order to reduce the separation between channels while increasing their bit-rate, further optical effects must be taken into account. After chromatic dispersion, so-called non-linear effects and polarization mode dispersion (PMD) are the main obstacles when tackling rates of 10 GBit/s (as required in the OC-192 standard) and higher. Non-linear effects such as stimulated Brillouin scattering, four-wave mixing, cross-phase and self-phase modulation dictate the maximum amplitude and minimum frequency spacing between channels, while PMD dictates the maximum data rate. In this thesis, we shall address only PMD.

1.1 Polarization Mode Dispersion

Single mode fibre supports two orthogonal polarization modes. In a perfectly circular core fibre, each of these modes experiences the same propagation delay. In real fibre, deformations from the ideal shape occur, resulting in a difference in the propagation speed of each of the two polarization modes. The associated difference in the propagation delays of these modes broadens any pulse sent through the fibre and impairs transmission. The difference in propagation delays is known as polarization mode dispersion. The extent of PMD within a fibre varies from manufacturer to manufacturer. It arises from fibre core deformations. Such deformations are inevitably produced during the fibre manufacture, but are also the result of stress on a fibre when it is packaged into a cable, and manipulated during cable laying operations.

PMD is mainly characterized by the differential group delay (DGD) between the fast and slow states of polarization (SOP). If this delay difference is a significant fraction

of a symbol period, then PMD can be expected to seriously degrade the performance of the transmission link over what it would be without PMD. For the non-return to zero (NRZ) binary data transmission schemes typically utilized in optical links, we can regard PMD to be a significant problem when the DGD approaches one-tenth of a bit duration, as a rule of thumb. In many fibre plants, the mean DGD does not exceed 40 ps, which is one tenth of an OC-48 bit-period. However, OC-192 transmission, with a bit duration of 100 ps, is jeopardized for fibres having a mean DGD of 40 ps or more.

While the DGD along a fibre is a fixed function at any instant, due to the random origins of the fibre geometric disturbances, over the ensemble of like fibres the DGD may be viewed as a random process evolving over time, wavelength, and various other parameters. With respect to time and wavelength, we can see that the DGD can be expected to be stationary (and thus would have a mean which does not vary with these parameters). The DGD has a Maxwellian distribution, which is uniquely characterized by its mean. The random nature of PMD also requires that the variation of DGD over time and wavelength be characterized, although the literature has neglected this aspect so far.

The PMD of a system consisting of a cascade of optical fibre components is a function of the PMD of each of its components. If we assume the statistics of the PMD of each subsystem to be statistically unrelated, then we can derive an expression for the PMD of the total system in terms of the PMD of the subcomponents. The validity of the assumption and thus the expression may be questioned.

1.2 Objective and Outline

The objective of this thesis is to characterize in detail the PMD of individual optical communications components, and the system which links them. Through measure-

ment, the mean DGD is estimated for the components and the system. The validity of the expression relating the PMD of cascaded links to the PMD of the link's constituents is thus to be verified.

This thesis is organized as follows: Chapter 2 gives a physical interpretation and mathematical representation of PMD in order to familiarize the reader with the concepts and terms required to discuss PMD. Chapter 3 analyses the statistical nature of the DGD variations over time and frequency, leading to the performance impact of DGD in a digital communications system.

Several methods of measuring PMD exist. The methods vary in their practicality and utility. Since the goal of this thesis cannot be attained without measurements, a discussion of the major PMD measurement techniques is given in Chapter 4. This includes some discussion of the intrinsic accuracy and experimental error inherent in the use of these techniques. From these possible techniques, a method is selected and then used for measurements of PMD reported in the subsequent sections of the thesis.

In order to estimate the findings of our cascaded link measurements, and to obtain certain parameters required in the statistical characterization of PMD, numerical simulations are desirable. The nature of these simulations and the model they are based upon are described, and their results are reported in Chapter 5.

Finally, a cascaded link system is designed and described in Chapter 6, based on available testing equipment, time, and devices / links. A methodology to characterize the PMD in the link is suggested, based upon findings from the simulations. The individual link components are then characterized in terms of PMD, followed by the entire link as a

whole. These results are compared with the expected overall link behaviour based on the PMD measurement of the individual links.

Chapter 2: Polarization Mode Dispersion

The general structure of an optical fibre is a core with a high index of refraction, surrounded by a lower index cladding. Transport fibre is made of fused silica with a refractive index of approximately 1.5. When a wave propagates along the fibre core and approaches the interface between the two mediums, the lower refractive index permits total internal reflection of the wave back towards the core. This is the basic principle of how a fibre serves as an optical waveguide.

An optical mode is a particular solution of the electro-magnetic wave equation which satisfies the boundary conditions pertinent to a propagation medium ([1], p. 32). Optical fibre modes can generally either be guided, such that they propagate with relatively little attenuation, or radiative, such that light is absorbed into the cladding. Multi-mode fibre has a wide core such that the wave equation has many guided modes. An applied signal will produce components in many or all of these modes. The different modes propagate along different spatially distributed paths, making full use of total internal reflection as shown in Figure 2.1. Since any two such paths will generally have different lengths, the wave-fronts of components along these two modes will arrive out of phase at the exit. The two modes effectively propagate at different speeds along the length of the fibre, and the disparity in arrival times of a signal is defined as multi-mode dispersion.

As the name suggests, single mode fibre (SMF) was developed to support only a single guided mode along which a light wave can travel successfully. The core of the SMF is made sufficiently small that the only solutions of the wave equation are (a) a guided mode and (b) multiple leaky modes. At the exit of the fibre, only the guided mode persists, as illustrated in Figure 2.1 (the curved lines represent wave-fronts). In the expressions

"multi-mode fibre" and "single mode fibre", the modes referred to are named "spatial modes" since the waves propagating along them can be thought of as taking different paths. The elimination of multi-mode dispersion through the use of SMF is key to high bit-rate digital communications.

Figure 2.1 Multi-Mode vs. Single Mode Fibre

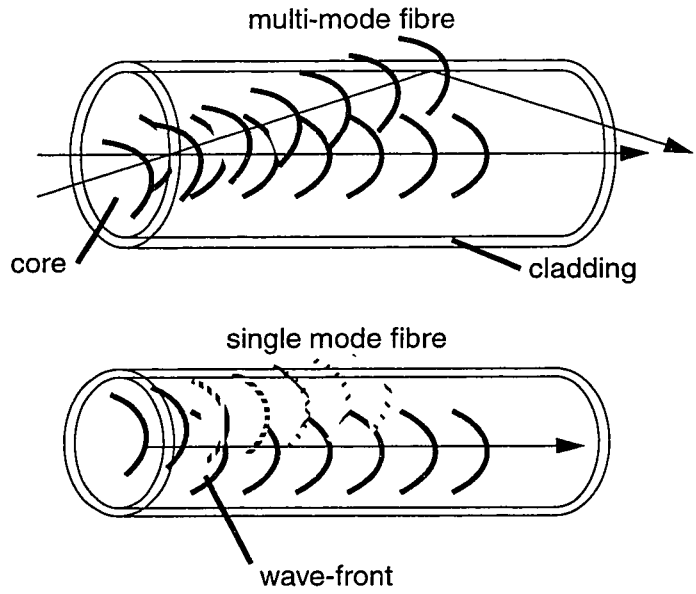

Nevertheless, even in a SMF, two orthogonal modes of polarization can still propagate. Thus, a single mode fibre in terms of spatial paths is actually a dual-mode fibre in terms of polarization paths. In a perfectly circular core fibre, both polarization modes have exactly the same group velocity. However, in a real fibre, deformations of the core geometry exist. Ellipticity in the fibre core causes birefringence, a difference in refractive index from one polarization mode to the other. Since the speed of light is inversely proportional to the index of refraction, a light wave containing components in both polarization modes launched at one end of the fibre will propagate with two different speeds, and the modes will arrive out of phase at the far end. This phase difference is the result of a propagation

delay difference which is the main effect of polarization mode dispersion. This effect is illustrated from a systems perspective in Figure 2.2. Naturally, this effect will cause signal degradation in a digital communications system.

Figure 2.2 Communications System Model

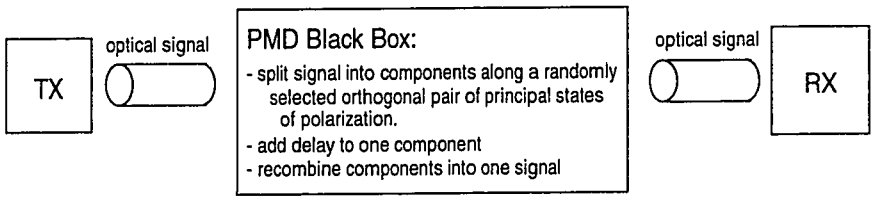

2.1 Physical Model

The geometric imperfections in the core are produced during the fabrication of the fibre. Other stresses are induced when single fibres are incorporated into the cable package, when the cable is laid, and when bending occurs. The fibre core is generally described by an ellipse. If one axis of the ellipse is greater than the other, and if the core cross-section maintains this constant shape over the entire fibre, two linear modes of polarization are supported. These modes are parallel to the axes of the ellipse, and have different indices of refraction, providing the basis of a polarization maintaining fibre for linear modes of polarization. This phenomenon is termed birefringence. In standard single mode fibre, birefringence occurs irregularly.

Furthermore, points of greater stress at random locations along the fibre cause the two polarization modes to scatter and couple again, a phenomenon termed random mode coupling. The geometry of the core in one section is generally uncorrelated with the geometry in an adjacent section separated by a mode coupling point, such that the core axes of the two sections are not lined up. The random mode coupling has the effect of mixing several modes of propagation. The effective principal states of polarization (PSPs) of a

long fibre having multiple random mode coupling points are no longer linear, even though the birefringent sections between two mode coupling points are said to have linear polarization modes.

Figure 2.3 shows the physical model of PMD within a single mode fibre. The birefringence in each section is characterized by the differential time delay $\Delta\tau$ between both polarization modes.

Figure 2.3 SMF Physical Model

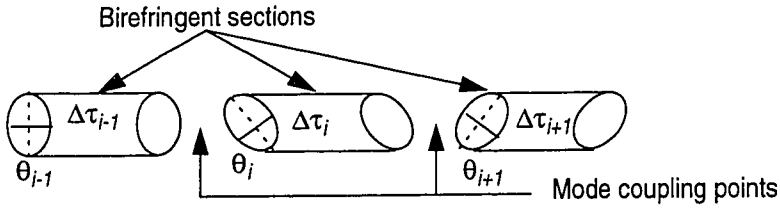

In this model, the axes in one section are randomly oriented with respect to the axes in the next section; in other words, the orientations from section to section are uncorrelated. From this assumption of uncorrelatedness between sections, the delays add up as the root sum of squares (RSS), i.e., the total differential group delay in a fibre is the square-root of the sum of the squares of the delays in all of its birefringent sections.

The above model is in fact a simplification of the birefringent structure in a real fibre. In uncorrelated sections within a fibre, the core geometry is generally not uniform over the length of each section, and as a result, the sections do not have uniform birefringence (i.e., with linear polarization modes). Furthermore, the frame of reference (the *XY* plane orthogonal to the propagation direction in Figure 2.3) is not static and can rotate in a random fashion about the propagation axis due to twists and bends in the fibre. Each section would then be described by incident and exit mode coupling angles.

In addition, mode coupling points are not always exact locations. If a fibre were to be cut into small enough sections, the orientation of the axes in adjacent sections would be shown to be correlated. However, as the distance between sections increases along the direction of propagation, the angle between the axes becomes less and less correlated, such that, on average, after a distance l, the mode coupling angles would be said to be essentially uncorrelated. The distance l is termed the average mode coupling length.

In the model described above, the average mode coupling length is the average length of a birefringent section, which also translates into the average distance between consecutive mode-coupling points. The length of a fibre L is characterized in general terms by its length with respect to the average mode coupling length l. A fibre can be long ($L >> l$,) short ($L << l$,) or of the order of l. The mode coupling length is not to be confused with the beat length, another term used in describing birefringence: in a uniformly birefringent medium, the beat length describes the length over which the phase in one polarization mode gains 2π over the phase in the orthogonal mode.

The use of simple uniform birefringence and equal incident and exit mode coupling angles in each section with respect to a fixed frame of reference gives rise to the same overall polarization effect as a more detailed account of a real fibre. The requirement for the additional section configuration data then becomes superfluous to the understanding of the phenomenon, and for this reason the simplification above is justified.

Another simplification used in the model of Figure 2.3 arises from the fact that, over wavelength, a section of fibre is more likely to have constant length than constant delay. The propagation delay between the two PSPs is caused by the birefringence or difference in index of refraction, which affects the velocity of propagation along the two

modes. If c_o is defined as the velocity of light in vacuum, λ is its wavelength, l_i is the length of a section, and n_X and n_Y are the indices of refraction along the X and Y axes, the differential delay $\Delta\tau_i$ is then given by:

$$\Delta\tau_i = \left|n_X(\lambda) - n_Y(\lambda)\right|\frac{l_i}{c_0}. \tag{2.1.1}$$

The index of refraction is known to vary with wavelength in standard fibre, which gives the delay $\Delta\tau_i$ in each section a dependence on frequency. Nevertheless, in fused silica between 1450 and 1600 nm (wavelength in vacuum), the index of refraction varies by less than +/-0.1%([30], p. 190). The birefringent refractive indices are expected to have similar frequency dependence, and therefore their difference will as well. Due to this negligible frequency dependence, the delay can be treated as constant over this wavelength range.

DGD is known to vary with time, or rather with environmental conditions which vary with time. From the model, there are only two degrees of freedom for each section: the differential delay $\Delta\tau_i$ and the mode coupling angle θ_i. Therefore, effects such as temperature and ambient pressure must affect either $\Delta\tau_i$, or θ_i, or both. To characterize the effects of environmental variables on the degrees of freedom of the model would be ideal, but to do so would require the determination of the polarization propagation properties along the entire length of a real fibre, which is generally not practical.

Two phenomena arise from the above model. The first one is evident from the model itself, in that the differential group delay at a particular wavelength varies with the length of the fibre: this can be seen as a random walk of the cumulative DGD $\Delta\tau(\omega_0)$ along the length of the fibre.

The other outcome, which is related to the random mode coupling, is variation of the DGD with frequency. With knowledge of the complete configuration of birefringent sections within a fibre length, one could determine the DGD variation over wavelength. However, the expression governing the variation becomes very complicated as soon as more than a few sections are considered. Furthermore, as stated earlier, the internal characteristics of the fibre are not known. Therefore, the DGD variation with frequency is more effectively treated as a random process.

As a random process, the DGD is partially characterized by its mean value with respect to frequency. As will be seen in Chapter 3, the mean is considered constant, and the instantaneous DGD has a Maxwellian distribution. Intuitively from the first outcome, the mean DGD will monotonically increase with the fibre length.

2.2 Jones Matrix Analysis

Jones matrix analysis enables the tracking of light polarization through a given medium. Any state of polarization can be expressed as a combination of components along orthogonal polarization states situated in a plane perpendicular to the direction of propagation. Horizontal (X-axis) and vertical (Y-axis) linear polarization states are convenient states for this purpose. A Jones vector (J_{in}) is a two dimensional complex vector which indicates the phases of arbitrary electric field components along the X and Y axes, respectively, denoted E_x and E_y. Often, the common phase of the Jones vector components are factored out, while the magnitude of the vector itself is normalized to unity.

The transmission characteristics of a medium such as a single mode fibre can be represented by a complex Jones matrix T, which can incorporate the various delays (translated into complex exponential phase terms) along the two input linear polarization axes.

The output polarization of a light wave propagating through a fibre is the product of the transmission Jones matrix by the input Jones vector:

$$\overrightarrow{J_{in}} = \begin{bmatrix} E_x \\ E_y \end{bmatrix}, \tag{2.2.1}$$

$$T = \begin{bmatrix} a & b \\ c & d \end{bmatrix}, \text{ and} \tag{2.2.2}$$

$$\overrightarrow{J_{out}} = T \cdot \overrightarrow{J_{in}} = \begin{bmatrix} a & b \\ c & d \end{bmatrix} \cdot \begin{bmatrix} E_x \\ E_y \end{bmatrix} = \begin{bmatrix} aE_x + bE_y \\ cE_x + dE_y \end{bmatrix}. \tag{2.2.3}$$

A birefringent section such as shown in Figure 2.3 can be written as a transmission matrix with a phase difference between X and Y states corresponding to the differential time delay $\Delta\tau_i$ [5], with a similarity transformation to rotate the delay by the mode coupling angle with respect to the frame of reference [23]. The angle θ_i represents the angle between the slow linear axis (the axis to which the half-delay is added) and the horizontal axis:

$$T_i = \begin{bmatrix} \cos\theta_i & \sin\theta_i \\ -\sin\theta_i & \cos\theta_i \end{bmatrix} \cdot \begin{bmatrix} e^{j \cdot \frac{2\pi \cdot \Delta\tau_i/2 \cdot c}{\lambda}} & 0 \\ 0 & e^{-j \cdot \frac{2\pi \cdot \Delta\tau_i/2 \cdot c}{\lambda}} \end{bmatrix} \cdot \begin{bmatrix} \cos\theta_i & -\sin\theta_i \\ \sin\theta_i & \cos\theta_i \end{bmatrix}. \tag{2.2.4}$$

2.3 Polarization Eigen-Modes, Principal States of Polarization

Polarization mode dispersion is a frequency (or wavelength) dependent phenomenon. One manifestation of this phenomenon is that monochromatic light emitted at a fixed input state of polarization will propagate through the fibre and exit in some output state of polarization. As the frequency of the monochromatic light is varied, the output polariza-

tion state will also vary, even though the input state of polarization is fixed. This phenomenon is termed polarization dispersion.

In the absence of polarization dependent loss (PDL), Poole [25] defines the principal states of polarization (PSPs) of a single mode fibre as the two frequency dependent states of polarization which exhibit no dispersion to first-order at that frequency. An input set of PSPs has a corresponding output PSP set, and represents an orthonormal pair by which one can represent any SOP propagating through the single mode fibre. They are obtained by evaluating the eigenvectors of a system where the first-order dispersion is set to null.

From [25], the complex transfer matrix T of a single mode fibre may be represented by the product of a complex propagation exponential $e^{\beta(\omega)}$ with a unitary Jones matrix $U(\omega)$:

$$T(\omega) = e^{\beta(\omega)} U(\omega), \text{ where} \tag{2.3.1}$$

$$U(\omega) = \begin{bmatrix} u_1(\omega) & u_2(\omega) \\ -u^*_2(\omega) & u^*_1(\omega) \end{bmatrix}, \text{ and } |u_1|^2 = |u_2|^2 = 1. \tag{2.3.2}$$

The electrical field of a monochromatic wave transmitted through the SMF is:

$$\vec{E}_{out} = T(\omega)\vec{E}_{in}, \tag{2.3.3}$$

where the electrical field is represented by a Jones vector:

$$\vec{E}_{in,\,out} = \begin{bmatrix} E^x_{in,\,out} \\ E^y_{in,\,out} \end{bmatrix} = \varepsilon_{in,\,out} e^{i\phi_{in,\,out}} \hat{\varepsilon}_{in,\,out}. \tag{2.3.4}$$

With a constant input electrical field, and maintaining that $\frac{d\hat{\varepsilon}_{out}}{d\omega}$ is zero (no polarization dispersion), the solutions for the resulting eigenequation are sought:

$$U^{-1}U'\hat{\varepsilon}_{in} = ik\hat{\varepsilon}_{in} . \tag{2.3.5}$$

The eigenvectors $\hat{\varepsilon}_{in}$ are the principal states of polarization, while the differential group delay between the two modes is equal to the difference between the corresponding eigenvalues k:

$$k_{\pm} = \pm\sqrt{|u'_1|^2 + |u'_2|^2}\text{; and } \Delta\tau = k_+ - k_- = 2\sqrt{|u'_1|^2 + |u'_2|^2}. \tag{2.3.6}$$

2.4 Poincaré Sphere Representation

The Jones vector analysis is a convenient mathematical representation of the polarization properties of a system. Unfortunately it is difficult to visualize polarization properties from it. A more convenient representation for visualization purposes is provided by the Poincaré sphere. The Poincaré sphere is a sphere upon which any polarization state has a single geographical location. A polarization state can be expressed as a 3-dimensional unitary vector, called a Stokes vector, which is anchored on the origin of the Cartesian coordinates and points to a location on the Poincaré sphere of unit radius. Linear polarization is represented by the equator, while circular polarization is at the poles (right-hand circular at the North, left hand at the South). Regions between the right-hand pole and the equator contain all predominantly right-hand elliptical polarization states, and conversely for the left-hand hemisphere.

Any Jones vector $\overrightarrow{J_{in}} = \begin{bmatrix} E_x \\ E_y \end{bmatrix}$ can be mapped to a Stokes vector $\hat{s} = \begin{bmatrix} s_1 \\ s_2 \\ s_3 \end{bmatrix}$ using the transformations ([4], pp. 33-66):

$$s_1 = \frac{|E_x|^2 - |E_y|^2}{|E_x|^2 + |E_y|^2}, \tag{2.4.1}$$

$$s_2 = \frac{2\mathrm{Re}\{E_x E_y^*\}}{|E_x|^2 + |E_y|^2}\text{, and} \tag{2.4.2}$$

$$s_3 = \frac{2\mathrm{Im}\{E_x E_y^*\}}{|E_x|^2 + |E_y|^2}. \tag{2.4.3}$$

Figure 2.4 Poincaré Sphere

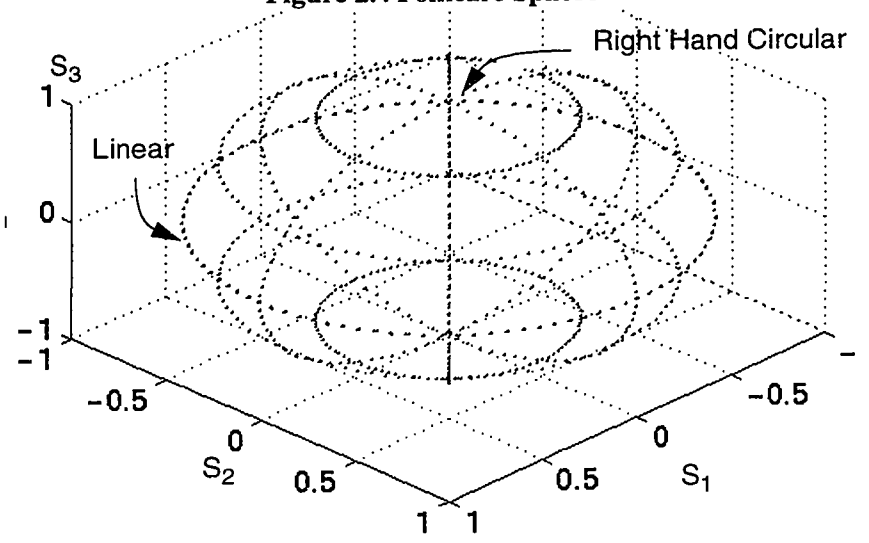

Orthogonal states of polarization (SOP) are always diametrically opposed on the sphere. When perturbing the frequency of an arbitrarily polarized input electrical field by a small amount, the Stokes vector representing the output SOP will draw an arc rotating around the diameter formed by the two PSPs [27].

In Jones notation, the PMD at a particular wavelength is characterized by a Jones vector indicating the fast output PSP (the PSP along which the delay is shortest), and a differential group delay $\Delta\tau(\omega)$. In Poincaré notation, it is convenient to use the PMD vector, whose orientation is that of the fast PSP and whose length is the DGD.

Chapter 3: Statistical Model

In all typical transmission applications, optical fibres are several orders of magnitude longer than the average mode coupling length. As a result, we can expect that the DGD of the fibre will exhibit a strong variation over wavelength (frequency). In this chapter, the DGD will be examined from a statistical perspective. The Maxwellian distribution which DGD samples adhere to will be described. Furthermore, the cascaded link rule of PMD will be explained, and the dependence of mean DGD on length will also be stated. The DGD variation with frequency will be described by a wide-sense stationary stochastic process, while this treatment will be justified. This chapter will also define the parameters used in this thesis to characterize the statistical variation of DGD with time and wavelength, and will summarize its impact on a digital communications system.

3.1 Maxwellian Distribution

The PMD vector is defined as the Stokes vector representing the fast output principal state of polarization, with magnitude equal to the DGD. The statistical description offered in the literature draws parallels with the Brownian motion of particles in a confined three-dimensional space [6], [9]. Similarly to a particle in a confined space, whose direction and speed becomes uncorrelated with its previous velocity, on average, after a mean correlation distance, the PMD vector also becomes uncorrelated in orientation and magnitude (which is equal to the DGD) after propagation down the fibre exceeding the mean correlation length, which, as described in Section 2.1, is equivalent to the average mode coupling length. The demonstration is lengthy, and beyond the scope of this thesis. The result is that all three dimensions of the Stokes PMD vector are identically distributed normal random variables with zero mean. A Maxwellian distribution describes the magni-

tude of a three-dimensional vector whose Cartesian coordinates constitute a set of independent, identically distributed, normal, zero-mean random variables.

The Maxwellian density function thus describes the probability density of obtaining a particular DGD in a fibre over wavelength and time if the mean DGD is known. The density function of a Maxwellian distribution is non-zero for positive values only, and is given by:

$$\rho_{\text{Maxwell}}(x, \mu) = \begin{cases} \frac{32}{\pi^2} \cdot \frac{x^2}{\mu^3} \cdot e^{-\frac{4}{\pi} \cdot \frac{x^2}{\mu^2}}, & x > 0 \\ 0, & x \leq 0 \end{cases}, \tag{3.2.1}$$

where μ is the single parameter of the distribution which is the mean of the distribution. The distribution is not symmetric (Figure 3.1) and so its median differs from the mean. We find that the first and second-order moments for a random variable X with this distribution are:

$$E\{X\} = \mu, \text{ and} \tag{3.2.2}$$

$$E\{X^2\} = \frac{3\pi}{8}\mu^2. \tag{3.2.3}$$

Of particular interest is the relation between the first and second moments:

$$\langle X^2 \rangle = \frac{3\pi}{8}\langle X \rangle^2, \text{ or } \mu = \langle X \rangle = \sqrt{\frac{8}{3\pi}\langle X^2 \rangle} \approx \frac{\sqrt{\langle X^2 \rangle}}{1.0854}. \tag{3.2.4}$$

Long optical fibres in typical telecommunications surroundings are subject to continuously changing environmental conditions over time. These variations are such that the ensemble of DGD characteristics of such a fibre over time equate to a statistical ensemble [11]. Reference [12] indicates that, provided the average mode coupling length is negligible with respect to the length of the fibre, DGD distributions over frequency

ensembles are equivalent to distributions over statistical ensembles, of which time ensembles are a subset. In a long optical fibre, the Maxwellian distribution describes the population of DGD samples at a particular wavelength over time, or, conversely, the population of DGD samples over frequency at a fixed instant in time. A mix of both populations will have the same distribution as either of the above.

Figure 3.1 Maxwellian Probability Density Function

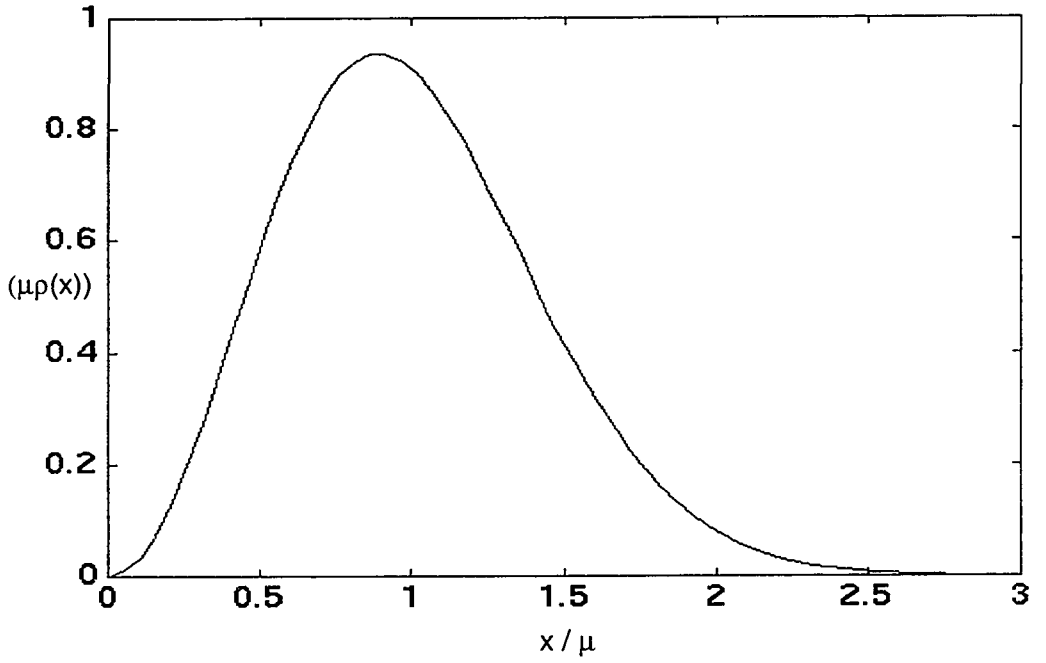

3.2 Cascaded Link Rule

As a general rule, vectors of random length and orientation add up as the root sum of squares: let Z_1 and Z_2 be two random processes representing the length of random vectors $\vec{V}_1$ and $\vec{V}_2$. Their vector sum is:

$$\vec{V}_{12} = \vec{V}_1 + \vec{V}_2, \tag{3.3.1}$$

while the length squared of $\vec{V}_{12}$ is given by:

$$Z_{12}^2 = Z_1^2 + 2Z_1Z_2\cos\theta + Z_2^2, \tag{3.3.2}$$

where θ is the angle between the two vectors. By assumption, the orientations of the vectors are uncorrelated, and thus the random angle θ between them is expected to have a uniform distribution between -π and +π. The mean value of $Z_{12}{}^2$ is:

$$\langle Z_{12}^2 \rangle = \langle Z_1^2 \rangle + 2\langle Z_1 Z_2 \rangle \langle \cos\theta \rangle + \langle Z_2^2 \rangle, \tag{3.3.3}$$

where <cosθ> evaluates to 0. This yields:

$$\langle Z_{12}^2 \rangle = \langle Z_1^2 \rangle + \langle Z_2^2 \rangle. \tag{3.3.4}$$

We can show that the PMD in concatenated fibre sections follows this quadratic rule. Using the Jones matrix analysis described in Section 2.2, at a particular frequency, two concatenated fibres have an arbitrary polarization transmission matrix with respect to each other, which can be described by [6]:

$$R = \begin{bmatrix} \cos\theta e^{-j\phi} & -\sin\theta e^{j\phi} \\ \sin\theta e^{-j\phi} & \cos\theta e^{j\phi} \end{bmatrix}. \tag{3.3.5}$$

Since a state of polarization can generally be described as elliptical, the angle θ represents the angle between the major axes of the two SOPs, while the angle φ is related to the difference in ellipticity from one SOP to the next. The above matrix R is transposed between the birefringence matrices of the two fibres, $M_{di} = \begin{bmatrix} e^{j\omega\Delta\tau_i/2} & 0 \\ 0 & e^{-j\omega\Delta\tau_i/2} \end{bmatrix}$, such that $(M_{d2})R(M_{d1})$ is the only matrix required in evaluating the DGD. It can be shown that the resulting DGD is given by [6]:

$$\Delta\tau_{12} = \sqrt{\Delta\tau_1{}^2 + \Delta\tau_2{}^2 + 2\Delta\tau_1\Delta\tau_2\cos 2\theta_{1-2}}, \tag{3.3.6}$$

where the physical interpretation of $2\theta_{1-2}$ is the angle between the Stokes output PSP of the first fibre and the Stokes input PSP into the second fibre.

If we consider two birefringent sections rather than two fibres, the orientation of the two Stokes PSPs mentioned above is constant over frequency, as is the DGD in each section. The DGD of the two concatenated sections is constant over frequency and equal to the value given by (3.3.6). However, based on the assumption stated in Section 2.1 that the angles between birefringent sections are random and uncorrelated, the resultant output PSP Stokes vector exhibits a rotation around the Poincaré sphere with frequency. The PSP rotates such that the angle $2\theta_{12\text{-}3}$ it makes with the input Stokes PSP of a third section then varies cyclically (i.e. a linear dependence on frequency with a range from 0 to 2π). The DGD of the three concatenated sections then has a periodic dependency on frequency:

$$\Delta\tau_{123}(\omega) = \sqrt{\Delta\tau_{12}{}^2 + \Delta\tau_3{}^2 + 2\Delta\tau_{12}\Delta\tau_3 \cos 2\theta_{12\text{-}3}(\omega)}. \qquad (3.3.7)$$

The fourth concatenated section would see a similar periodic variation over frequency of the angle $2\theta_{123\text{-}4}$ and of the DGD $\Delta\tau_{1234}$, although the variations with respect to frequency would no longer be as simplistic. As more and more sections are concatenated, the variation of the angle $2\theta_{1\ldots(n\text{-}1)\,\text{-}\,n}$ effectively becomes non-deterministic, such that the expression:

$$\Delta\tau_{1\ldots n}(\omega) = \sqrt{\Delta\tau_{1\ldots(n-1)}{}^2 + \Delta\tau_n{}^2 + 2\Delta\tau_{1\ldots(n-1)}\Delta\tau_n \cos 2\theta_{1\ldots(n-1)-n}(\omega)}, \qquad (3.3.8)$$

becomes increasingly difficult to evaluate, even if all of the section orientations are known. It is then easier to describe the variation of the DGD with frequency as a random process. If we consider a frequency ensemble (i.e., the resultant DGD at different frequencies), over a large enough wavelength range, the angle $2\theta_{1..(n\text{-}1)\,\text{-}\,n}$ has a uniform distribution from $-\pi$ to $+\pi$, such that the expected value of $\cos 2\theta_{1..(n\text{-}1)\,\text{-}\,n}$ averaged over wavelength is 0. For n sections, the frequency average of expression (3.3.8) becomes:

$$\langle \Delta\tau_{1\ldots(n-1)n}{}^2 \rangle = \langle \Delta\tau_{1\ldots(n-1)}{}^2 \rangle + \Delta\tau_n{}^2 . \tag{3.3.9}$$

If n is sufficiently large that the variation of 2θ can be perceived as a random process over wavelength, and that the DGDs of the first few sections are negligible with respect to the DGD of the entire link, the mean square DGD of the entire link can be approximated as:

$$\langle \Delta\tau_{1\ldots n}{}^2 \rangle = \sum_{i=1}^{N} \Delta\tau_i{}^2 . \tag{3.3.10}$$

Let us now consider a frequency ensemble of a concatenation of two fibre lengths made of multiple sections. From the explanation given above and the statement made in Section 2.4, we can assume that the PSP orientations of the two fibre lengths vary with wavelength in a random fashion. From (3.3.6), and assuming that the DGDs $\Delta\tau_i$ are independent of the angle θ, we find that, over wavelength:

$$\langle \Delta\tau_{12}^2 \rangle = \langle \Delta\tau_1{}^2 \rangle + \langle \Delta\tau_2{}^2 \rangle . \tag{3.3.11}$$

Equation (3.3.11) is an extension of (3.3.10), since $\langle \Delta\tau_1{}^2 \rangle$ and $\langle \Delta\tau_2{}^2 \rangle$ can be broken down into the sum of the squares of the differential delays of their constituent sections.

An ensemble of identical concatenations at fixed frequency (as opposed to a frequency ensemble), made of fibres with the same mean squared DGD as above ($<\Delta\tau_1{}^2>$ and $<\Delta\tau_2{}^2>$), will have an ensemble mean with the same result, provided that we adhere to the assumption that the orientation of the two PSPs are uncorrelated from concatenation to concatenation.

Equation (3.3.11) can further be extended to relate the mean DGD of a larger cascaded link to the mean DGDs of the constituent spans, and is known as the cascaded link rule. Assuming long fibres made up of numerous sections (high mode coupling), the DGD of the link will have a Maxwellian distribution. Since the second moment of a Maxwellian

distribution $\langle \Delta\tau^2 \rangle$ is proportional to the square of the mean $\langle \Delta\tau \rangle^2$ as stated in (3.2.4), the cascaded link rule can be written:

$$\langle \Delta\tau \rangle^2_{\text{casc}} = \sum_{i=1}^{N} \langle \Delta\tau \rangle_i^2 . \tag{3.3.12}$$

3.3 Dependence on Length

If the fibre length is lower than, or in the same order as, the average mode coupling length, the fibre is in the short length regime, and the total differential group delay varies directly with the length. This only applies for very short lengths of fibre, typically less than 1 km long [10]. If, however, the length is much larger than the average mode coupling length (long length regime), the mean DGD varies with the square root of the length.

Using the physical model, a fibre is made up of several sections of varying birefringence, coupled at uncorrelated angles. According to (3.3.10), a fibre made up of N uncorrelated sections concatenated together would have a mean DGD of:

$$\overline{\Delta\tau^2}_{\text{Fibre}} = \sum_{i=1}^{N} \Delta\tau_i^2 \cong N\overline{\Delta\tau^2}_{\text{section}} , \tag{3.4.1}$$

where $\overline{\Delta\tau^2}_{\text{section}}$ is the mean square section DGD. However, it is reasonable to assume that the length L is proportional to the number of sections, $L \propto N$, since sections can be characterized by the average mode coupling length l. Also, from (3.2.4), for a Maxwellian distribution, the mean is proportional to the square-root of the second-moment, $\langle X \rangle \propto \sqrt{\langle X^2 \rangle}$. Developing the above proportionalities into multiplications by constants k_1, k_2 and k, we get:

$$\overline{\Delta\tau} = k_1\sqrt{\overline{\Delta\tau^2}} = k_1\sqrt{\overline{\Delta\tau^2}_{\text{section}}}\sqrt{N} = k_1\sqrt{\overline{\Delta\tau^2}_{\text{section}}}\sqrt{k_2}\sqrt{L} = k\sqrt{L}. \tag{3.4.2}$$

Therefore, assuming the DGD of the fibre adheres to a Maxwellian distribution, the square

of the mean DGD of the fibre is proportional to the fibre length L, and the mean square DGD.

Although the dependence on length has been established based on the assumptions stated above, the expression can further be simplified by relating the mean DGD directly to the mean section delay. The section differential delay is defined as the delay between the fast and slow axes of a section, and is always positive. It is reasonable to assume that the population of section differential delays within a fibre will have a normal distribution with positive mean, and some given variance. The standard-deviation σ of the delay is defined by the following expression:

$$\sigma^2 = E\{(\Delta\tau_{section} - \overline{\Delta\tau}_{section})^2\} = \overline{\Delta\tau^2}_{section} - (\overline{\Delta\tau})^2_{section}. \qquad (3.4.3)$$

If σ is expressed as a fraction η of the mean $\overline{\Delta\tau}_{section}$, then the mean of the square is related to the square of the mean by:

$$\overline{\Delta\tau^2}_{section} = (\overline{\Delta\tau})^2_{section} + \sigma^2 = (1+\eta^2)(\overline{\Delta\tau})^2_{section}. \qquad (3.4.4)$$

Therefore, the means of squared differential delays $\overline{\Delta\tau^2}_{Fibre}$ and $\overline{\Delta\tau^2}_{section}$ are proportional to the squares of the means $(\overline{\Delta\tau})^2_{Fibre}$ and $(\overline{\Delta\tau})^2_{section}$ respectively. From the assumptions stated above, the mean fibre DGD is related to the fibre length and to the mean section DGD by:

$$\overline{\Delta\tau}_{Fibre} = \sqrt{k_3 L}\,\overline{\Delta\tau}_{section} = k\sqrt{L}, \qquad (3.4.5)$$

where k is the fibre PMD coefficient, which takes into account the mean section delay. The PMD coefficient (typically in units of $ps/\sqrt{km}$) is often used by manufacturers to specify the maximum expected PMD in their fibres, or by systems engineers to specify the maximum tolerable PMD for fibres used in a communications system.

The square-root dependency on length is treated in more detail in references [6], [19], [26], and [29]. The direct relation between mean fibre DGD and mean section DGD is used in numerical simulations discussed in Chapter 5.

3.4 Stationarity

The literature to date pertaining to prolonged measurements of DGD in fibre samples has described the mean DGD of a fibre as remaining constant (within statistical fluctuation) over time, and over different wavelength ranges [7], [10], [14], [32].

A wide-sense stationary stochastic process over frequency is a process with a constant mean, and an autocorrelation function, $R_\omega(\omega_1, \omega_1 + \Delta\omega)$ which is dependent only on the separation in wavelength $\Delta\omega$. For convenience, analysis can be conducted over wavelength rather than frequency, using $R_\lambda(\lambda_1, \lambda_1 + \Delta\lambda)$. Similarly, a process can be declared wide-sense stationary over time if the mean over time is constant, and the autocorrelation $R_t(t_1, t_1 + \Delta t)$ is dependent only on the difference in time Δt.

If we consider a frequency ensemble of fibres (a single fibre at different wavelengths), the development in Section 3.2 gives the expression for the ensemble average of the DGD (3.3.10). This average does not depend on the frequency range, but on the constituent fibre sections. The literature further supports that the mean DGD remains constant regardless of the wavelength range it is measured over (within statistical fluctuation) [7], [10], [14], [32]. Furthermore, although the autocorrelation function over frequency of the DGD process can only be estimated due to the limited wavelength range over which the DGD is obtained through measurement, it has a fixed characteristic (FWHM), as will be discussed later, which is dependent on the mean DGD. It is thus reasonable to hypothesize

that the DGD variation with frequency can be described by a wide-sense stationary process.

If we consider an ensemble of identically made fibres at a given frequency, i.e., fibres with an identical set of birefringent sections, but with a different set of mode coupling angles from one fibre to the next (similar to the concatenation ensemble used in Section 3.2), the mean of the DGDs of these fibres would be given by (3.3.10). Such an ensemble of fibres is not physically realistic: how would one guarantee the same set of birefringent sections in separately manufactured fibres? However, with some assumptions, this ensemble can be used to represent a given fibre at different instants in time.

This representation varies only one of the two degrees of freedom ($\Delta\tau_i$, θ_i) mentioned in Section 2.1. Varying environmental conditions have an effect on the PMD in a fibre, and are known to change the DGD-wavelength characteristic over time. Conditions such as temperature, ambient pressure, etc., exert fluctuating stresses along the length of a fibre. These stresses can affect mode coupling points (causing a change in the mode coupling angles, $d\theta_i$) but can also induce birefringence (causing changes in the section differential delay $d\Delta\tau_i$). Since, as mentioned above, the literature indicates that the mean DGD of a fibre remains constant within some acceptable fluctuation, and since (3.3.10) relates the mean DGD only to the section differential delays ($\Delta\tau_i$), it is reasonable to assume that variation in the section birefringence ($d\Delta\tau_i$) is negligible with respect to variation in the mode coupling angles ($d\theta_i$).

The assumption of sections of constant birefringence and the findings stated in the literature lend support to the first condition of constant mean over time. Unfortunately, environmental conditions do not vary uniformly over time. Therefore, the autocorrelation

function of DGD over time will be dependent on both time t and the difference in time Δt. The variation of DGD over time cannot be said to be wide-sense stationary.

Nevertheless, from the assumption of wide-sense stationarity of the DGD process over frequency, coupled with the assumption of constant mean over time, it is reasonable to expect that mean DGDs averaged over frequency will be constant over time.

3.5 Characterizing the Distribution

To characterize any statistical distribution, the first and second moments (mean and variance) are useful, although incomplete, indicators. For a Maxwellian distribution, as stated earlier, the mean uniquely characterizes the distribution. The standard deviation is directly related to the mean, and, from (3.2.4), is given by:

$$\sigma = \sqrt{\frac{3\pi}{8} - 1}\ \mu \cong 0.4220\,\mu\,. \tag{3.5.1}$$

In practice, the ratio of standard-deviation to mean can be compared to the theoretical value 42.2% as a quick and simple metric to ensure consistency with the Maxwellian distribution.

For assessment of impairments in digital communications, two other important notions are desired to characterize the DGD process. DGD varies in a continuous yet non-deterministic fashion with both time and frequency. Therefore, it is useful to describe the variation of DGD with respect to each of these variables. Due to the random nature of the variation, it is best described by determining how far in time or in wavelength the DGD becomes uncorrelated with a given starting point.

3.5.1 Correlation Bandwidth

DGD is a continuous function over frequency (wavelength). Broadly, the DGD at frequencies close to one another is strongly correlated while larger separations produce correlations close to zero. A measure of the correlation behaviour is provided by the correlation bandwidth[1] $\Delta\omega_c$ or, in terms of wavelength, $\Delta\lambda_c$. To evaluate $\Delta\lambda_c$, the normalized autocovariance function $C_\lambda(\Delta\lambda)$ of a plot of DGD over wavelength must be computed, where $C_\lambda(\Delta\lambda)$ is given by:

$$C_\lambda(\Delta\lambda) = \frac{\int_0^\infty (\Delta\tau(\lambda) - \overline{\Delta\tau})(\Delta\tau(\lambda + \Delta\lambda) - \overline{\Delta\tau})d\lambda}{\int_0^\infty (\Delta\tau(\lambda) - \overline{\Delta\tau})^2 d\lambda}, \tag{3.5.2}$$

where $\Delta\tau(\lambda)$ is the instantaneous DGD at wavelength λ.

Based on the assumption of a long fibre containing numerous birefringent sections, periodicity in the process is hidden over a finite wavelength range because of the complexity of the expression for the resultant Jones transmission matrix at each wavelength. The DGD function $\Delta\tau(\lambda)$ is effectively non-deterministic. For this reason, the autocovariance function will only contain one peak centred around a wavelength separation 0, and can therefore be used for correlation bandwidth analysis.

Define $\Delta\lambda_c$ as the full-width at half-maximum (FWHM) of $C_\lambda(\Delta\lambda)$:

$$\Delta\lambda_c \Rightarrow C_\lambda(\frac{\Delta\lambda_c}{2}) = \frac{1}{2}. \tag{3.5.3}$$

The notion of autocorrelation width in PMD was introduced in [24]. Empirically, this cor-

1. In the neighbourhood of a given wavelength, a frequency bandwidth is approximately proportional to a wavelength separation. A spacing of 1 GHz is equivalent to ~8 pm around 1550 nm, and the relation holds true to within +/-12.5% over the range 1450-1600 nm. Since frequency and wavelength are equivalent, the term "bandwidth" will be used to describe a difference in frequency *or* in wavelength, and is commonly used in the field of optical communications, particularly in dealing with wavelength division multiplexing applications.

relation bandwidth is believed to be related to the mean DGD by:

$$\Delta\omega_c\overline{\Delta\tau} = k_\omega \text{ [1]}, \text{ or, near a specific wavelength: } \Delta\lambda_c\overline{\Delta\tau} = k_\lambda . \qquad (3.5.4)$$

Within this thesis, k_ω and k_λ are referred to as the correlation bandwidth constants with respect to frequency and wavelength.

The relation (3.5.4) suggests a reciprocity between the mean DGD and the frequency range over which the DGD is considered. The term "reciprocal window size" will indicate, for various DGD processes, the product of mean DGD by the frequency range over which the process is considered. Windows of different DGD processes but constant reciprocal window sizes have statistically equivalent variation within their respective frequency ranges.

3.5.2 Correlation Time

Similarly, the instantaneous DGD at a particular wavelength and time t is correlated with the DGD at time $t+\Delta t$ if $|\Delta t|$ is less than Δt_c, the correlation time, and uncorrelated otherwise. To evaluate Δt_c, a function similar to $C_\lambda(\Delta\lambda)$ can be computed:

$$C_{t,\lambda_1}(\Delta t) = \frac{\int_{-\infty}^{\infty}(\Delta\tau_{\lambda_1}(t)-\overline{\Delta\tau})(\Delta\tau_{\lambda_1}(t+\Delta t)-\overline{\Delta\tau})dt}{\int_{-\infty}^{\infty}(\Delta\tau_{\lambda_1}(t)-\overline{\Delta\tau})^2 dt} . \qquad (3.5.5)$$

However, if many DGD values at different wavelengths are known, the cross-correlations of the entire scans can be used to provide an average correlation time over all sampled wavelengths:

---

1. $\Delta\omega_c$ is the frequency correlation bandwidth in radians/s (i.e. divide by 2π for the value in Hz).

$$C_t(t) = \frac{\int_{-\infty}^{\infty}\int_{0}^{\infty}(\Delta\tau(\lambda, t) - \overline{\Delta\tau})(\Delta\tau(\lambda, t + \Delta t) - \overline{\Delta\tau})d\lambda dt}{\int_{-\infty}^{\infty}\int_{0}^{\infty}(\Delta\tau(\lambda, t) - \overline{\Delta\tau})^2 d\lambda dt}. \quad (3.5.6)$$

We define Δt_c as the FWHM of $C_t(\Delta t)$:

$$\Delta t_c \Rightarrow C_t(\frac{\Delta t_c}{2}) = \frac{1}{2}. \quad (3.5.7)$$

In practice, of course, evaluating such integrals over an infinite range is impossible. The limits of the integrals are replaced with starting and ending times and wavelengths, while the integrations are replaced by summations. The same equation can be used to establish the correlation temperature, by varying the temperature of a device between measurements, and by replacing t with T in (3.5.6). The notion of cross-correlating DGD instances over temperature was introduced in [16], where DGD wavelength scans were correlated against a reference scan.

3.6 Impact on System Performance in a Digital Communications System

The importance of PMD is in its degradation of an optical communications system. The goal of reducing the number of spatial modes in a fibre to one (as in a single mode fibre) is to reduce the number of paths along which an optical signal can travel within the same optical channel. The dispersion seen when many paths with different optical lengths are taken is called multi-mode dispersion. As we have seen, however, even single mode fibre allows two polarization modes which generally do not have the same optical length.

If the effect of PMD were static, a fixed equalizer taking into account the delay between the two paths could be used to "straighten out" the signal. However, the DGD and

PSPs vary with time. The received signal then exhibits fading, not unlike that in a wireless, multi-path medium.

When designing an optical communications link, it is common practice to evaluate a link budget taking into account the system in a piecemeal fashion. The link budget informs the engineer of what signal level will have to be transmitted into the link, how and where to add amplifiers and regenerators in the fibre plant, to achieve with assurance a required bit-error rate (BER) at the receiver. Attenuation or loss in a fibre is taken into account by measuring the fibre loss, adding a margin to cover effects of aging, and directly subtracting this "penalty" from the transmission power. Other effects are not as easy to account for. In general, however, an effect can be directly translated into a quality factor, or power difference in dB, called "penalty", which must be added to the transmit end in order to achieve a desired maximum bit-error rate (BER). The mapping between the extent of this effect and the penalty is done analytically where possible, and is supported empirically by measuring the receive power required to maintain a certain BER while controlling the effect in question.

To analytically derive the penalty which will be applied due to PMD, the literature to date attempts to measure pulse distortion occurring under various levels of PMD. An important factor is the proportion of the components travelling parallel to each PSP. In terms of electric field, using Jones analysis [2]:

$$\vec{E}_{out}(t) = \vec{E}_{in} e^{(-\alpha + j\psi(\omega) + j\omega t)} \times [(\hat{e}_{in} \cdot \hat{\varepsilon}_{in}^{+*}) \exp(j\Delta\phi/2)\hat{\varepsilon}_{out}^{+} + (\hat{e}_{in} \cdot \hat{\varepsilon}_{in}^{-*}) \exp(-j\Delta\phi/2)\hat{\varepsilon}_{out}^{-}] \quad , \qquad (3.6.1)$$

where ω is optical frequency, α a loss, and $\psi(\omega)$ a phase factor. The normalized Jones vector $\hat{e}_{in}$ represents the launch state of polarization into the fibre, while the vectors $\hat{\varepsilon}_{in}^{+/-}$ and

$\hat{\varepsilon}^{+/-}_{out}$ are the slow (+) and fast (-), input and output PSPs respectively. The DGD is implicit in the exponential phase $\Delta\phi = \omega \cdot \Delta\tau(\omega)$. Of course, the above equation does not take into account variation of DGD and PSP with frequency. If we consider the terms $\exp(\pm j\Delta\phi(\omega_0)/2) \cdot \hat{\varepsilon}^{+/-}_{out}(\omega_0)$, which are exponential versions of the PMD vector, we can expand them into a Taylor series to second-order around the carrier frequency ω_0; the exponential PMD term becomes:

$$\exp\left(\pm\frac{j\Delta\phi(\omega)}{2}\right)\varepsilon^{\pm}_{out}(\omega) \cong \exp\left(\frac{\pm j\Delta\phi(\omega_0)}{2}\right)\varepsilon^{\pm}_{out}(\omega_0) \pm$$
$$j\frac{\Delta\omega}{2}\frac{d\phi}{d\omega} \cdot \exp\left(\frac{\pm j\Delta\phi(\omega_0)}{2}\right) \cdot \varepsilon^{\pm}_{out}(\omega_0) + \Delta\omega \cdot \exp\left(\frac{\pm j\Delta\phi(\omega_0)}{2}\right) \cdot \frac{d}{d\omega}\varepsilon^{\pm}_{out}(\omega_0) \quad .(3.6.2)$$

The first term on the right hand side represents first-order PMD: the splitting of the wave into its two PSPs each with its respective delay. The two other terms represent the second-order PMD which are dependent on the variation of DGD and PSP with frequency.

3.6.1 First-Order Effects

As seen above, the effects of differing birefringence and mode coupling over both polarization modes is more than just a delay between pulses travelling in the two modes. The delay is only the first-order effect, but is the most important one in digital communications systems. Therefore, without equalization, and assuming equal power is transmitted along both polarization modes, as a rule the delay should be less than some fraction of the bit period (mean delay less than 1/10th [15], instantaneous delay less than 1/4 [8]) to keep the impact on the BER to acceptable levels. Using the 1/10th rule, at OC-48 rates (2.5 Gbit/s), the mean delay must be less than 40 ps, while at OC-192 (10 Gbit/s), the mean DGD must be less than 10 ps. The exact fraction does not apply to all receivers, as some may compensate for the delay distortion to reduce the impact or BER. Nevertheless,

the rule provides a good bench-mark for evaluating threshold situations for an optical communications system.

If $P_{in}(t)$ represents the power of a pulse sent down the fibre, it has power component coefficients γ along the fast and (1-γ) along the slow PSPs, which are respectively advanced and delayed by $\Delta\tau/2$ at the output [22]:

$$P_{\text{out}}(t) = \gamma P_{\text{in}}(t - \frac{\Delta\tau}{2}) + (1-\gamma)P_{\text{in}}(t - \frac{\Delta\tau}{2}), \text{ where} \tag{3.6.3}$$

$$\gamma = \left\| \hat{e}_{\text{in}} \cdot \hat{\varepsilon}_{\text{in}}^{*} \right\|^2. \tag{3.6.4}$$

The superposition of two delayed components causes a pulse broadening with respect to the initial pulse width. The effect is intuitively dependent on the amount of power launched in each state. One reference [22] estimates this penalty to be:

$$\text{penalty(dB)} \approx 26\frac{\Delta\tau^2\gamma(1-\gamma)}{T_b^2}, \tag{3.6.5}$$

where T_b is the bit length. Since $\Delta\tau$ varies with time and wavelength, it may be more useful to give a penalty based on the expected (mean) $\Delta\tau$:

$$\text{penalty(dB)} \approx 5.1\left(\frac{\overline{\Delta\tau}}{T_b}\right)^2. \tag{3.6.6}$$

Reference [3] finds a similar result while evaluating the probability of occurrence of a particular penalty given the mean penalty. Additionally, it states that the variance of the penalty is approximately as large as the mean penalty. The mean penalty functions shown below agree to some extent. The important common point is the square-law dependency of penalty on mean DGD.

Figure 3.2 PMD Penalty

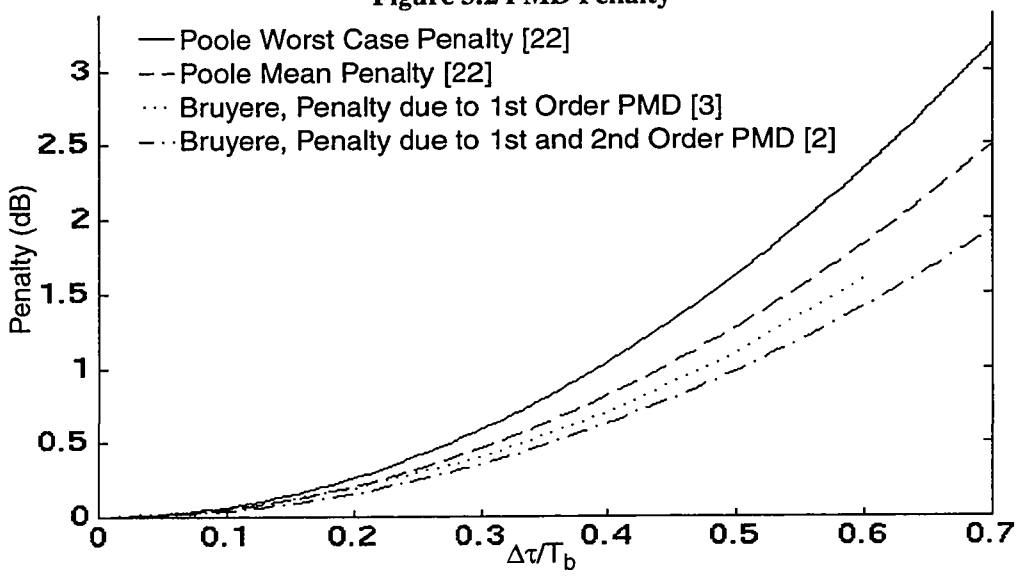

3.6.2 Second-Order Effects

Since the DGD $\Delta\tau(\omega)$ varies with wavelength, the phase factors $\exp(\pm j\Delta\phi(\omega)/2)$ in (3.6.2) also vary over the signal bandwidth $\Delta\omega$. Furthermore, the larger the signal bandwidth, the more the two PSPs $\hat{\varepsilon}_{in}^{\pm}$ will suffer dispersion over the band occupied by the signal. The expressions $(\hat{e}_{in} \cdot \hat{\varepsilon}_{in}^{\pm *})\exp(\pm j\Delta\phi(\omega)/2)$ in (3.6.1) thus have two wavelength dependent terms: $\Delta\phi(\omega)$ and $\hat{\varepsilon}_{in}^{\pm}(\omega)$, the "second-order" effects. These two effects have different impacts on the signal degradation.

Reference [2] indicates that the instantaneous penalty is highly dependent on the input state of polarization with respect to the input PSP. It also concludes that the frequency dependence of the DGD has little influence on the penalty compared to the frequency dependence of the PSPs. Nevertheless, in a fibre with random mode coupling, the DGD, its derivative with respect to frequency, and the rotation of the PSPs with frequency are statistically related [2].

Based on the assumption stated in Section 3.5.1 that the correlation bandwidth is inversely proportional to the mean DGD, fibres with high mean DGD have a smaller correlation bandwidth than fibres with low mean DGD, and must therefore exhibit more DGD variation over wavelength: the phase factor in (3.6.2) varies more for high PMD fibres. The rate of PSP rotation over wavelength is similarly related to the mean DGD. In [2], the "PSP bandwidth" is defined as the bandwidth over which the contributions of the second-order terms in (3.6.2) are less than 10% of the first-order terms, and is also inversely proportional to the mean DGD. In simple terms, fibres with low mean DGD have relatively constant DGD and PSP over small frequency perturbations, while fibres with high mean DGD exhibit greater variation of DGD and PSP over the same frequency intervals. Figure 3.3 and Figure 3.4 below illustrate this variation for numerically simulated fibres[1] of mean DGD 2 ps and 20 ps over a ±40 GHz frequency window centred around 1550 nm. At OC-192 rates, second-order PMD effects become significant for links with mean DGD values above 5 ps [2], although an experimental investigation indicates that links of mean DGD less than 10 ps are not likely to suffer second-order PMD impairments [15].

1. These numerical simulations were performed in the scope of this thesis, and are further described in Chapter 5.

Figure 3.3 Evolution of DGD for Simulated Fibres

Evolution of DGD for 2 ps Fibre

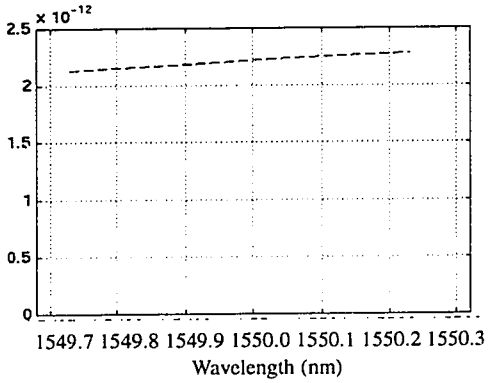

Evolution of DGD for 20 ps Fibre

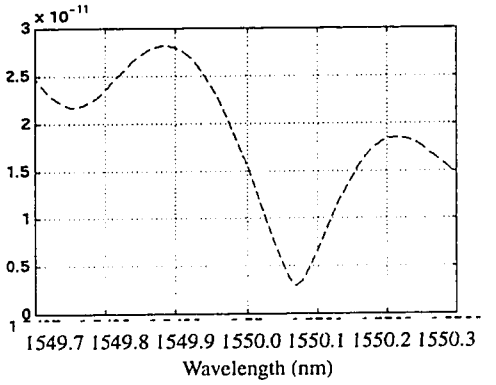

Figure 3.4 Evolution of PSP for Simulated Fibres

Evolution of PSP for 2 ps Fibre

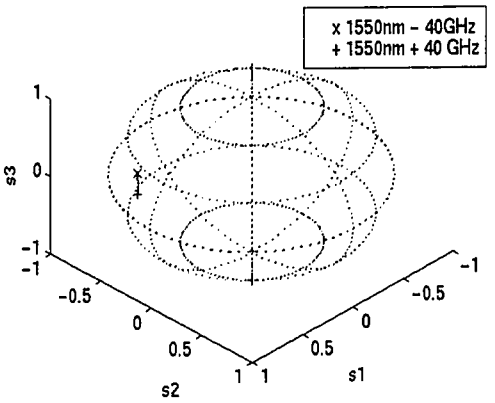

Evolution of PSP for 20 ps Fibre

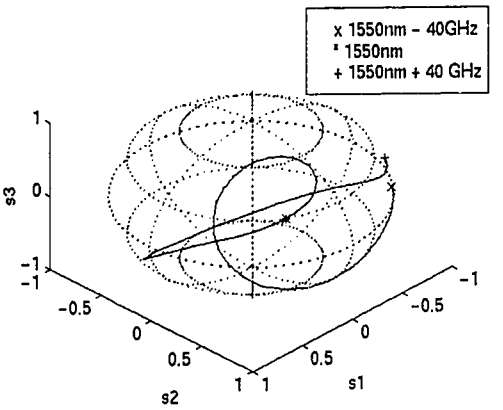

From the relation between the three variables (PMD vector and its derivatives), the expected mean penalty due to combined chromatic and first and second-order polarization dispersion amount to the empirical result [2]:

$$\langle P \rangle [\mathrm{dB}] \approx 268\left(\frac{1}{2}\frac{\ddot{\beta}_0 z}{T_{\mathrm{bit}}^2}\right)^2 + \frac{40}{3}\cdot\frac{\langle \Delta\tau^2 \rangle}{4T^2_{\mathrm{bit}}}\ , \qquad (3.6.7)$$

where $\ddot{\beta}_0$ is the chromatic dispersion. This result is compared with first-order effects in Figure 3.2. Although the mean penalty due to both first and second-order does not show any increase with respect to the penalty due to first-order PMD[1] only, the standard deviation of the penalty due to second-order PMD surpasses the mean penalty, and increases as a function of the amount of chromatic dispersion present in the fibre [2].

3.6.3 Correlation Time, Temperature

As mentioned in Section 3.5, the correlation time and bandwidth play an important role in assessing the penalty in an optical communications system.

As a note, time on its own does not directly affect the mode coupling aspects of a SMF. However, environmental conditions such as temperature, ambient pressure, wind and earth movement, which do vary with time, can cause PMD variation. Since these environmental conditions vary from day to day, and since the combinations of their occurrences are not likely to be reproduced or even completely measured, it is much more convenient to measure correlation over time than any other variable. The correlation time can be thought of as the duration of a particular DGD value at a fixed wavelength (an "event").

3.6.4 System Lifetime

Given the expected lifetime of a system and the duration of an instance (correlation time), the number of instances over the lifetime is a straight-forward calculation. Furthermore, with knowledge of the distribution of the DGD and the DGD above which a certain penalty will be incurred, and defining an "event" as an instance during which a

1. The expressions estimating penalty due to first-order only PMD pre-date the combined second-order expression. The penalty was revised in the later publication, such that the penalty estimate due to first-order only PMD shown on the graph was reduced as shown in the expression estimating the combined PMD penalty.

wavelength channel will be subject to such a penalty, one can evaluate the number of events in a year, or over the system lifetime, where the system will be incapacitated due to DGD exceeding the tolerable amount.

Chapter 4: Measuring PMD

To date several methods have been devised to measure the PMD within an optical fibre component. These methods vary in complexity and utility. Three methods will be discussed here, namely the Jones matrix eigen-analysis method, the wavelength scanning method and the interferometric method. The theory behind them, the equipment setup, dynamic range and step size will be discussed, and typical results from their application given. The measurement error associated with these methods as well as the statistical fluctuation intrinsic to PMD measurements are reported from the literature pertaining to PMD measurements. Based on the latter fluctuation, an expression is given to test the real-world validity of a DGD measurement, knowing the bandwidth over which the measurement is taken. The goodness of fit test used on the measured distributions is also explained.

4.1 Jones Matrix Eigen-Analysis

4.1.1 Theory

The Jones matrix eigen-analysis (JME) method characterizes the PMD in a fibre by directly measuring its transmission characteristics at a set of equally spaced wavelengths in a given wavelength range [28]. As discussed in Section 2.2, the polarization effects of any transmission medium can be mathematically modelled by a Jones matrix. The Jones matrix at a particular wavelength is a 2 x 2 matrix, and so in principle it can be determined with two known input and corresponding output polarization states, each represented by a Jones vector. Unfortunately, measurement errors can lead to large errors in the determined Jones matrix. However, by sending three differently polarized beams of light and again measuring the output polarization, the transmission medium's Jones matrix may be numerically evaluated in a fashion more tolerant to experimental error. The proc-

ess may be repeated over a range of wavelengths so as to characterize the medium over a desired frequency spectrum. By computing the difference between matrices of adjacent wavelengths, a frequency derivative of the matrices is approximated, and can be used to compute the desired eigenvalues and vectors of (2.3.5). The phase between eigenvalues is easily translated into a delay, namely the DGD between PSPs. The actual eigenequation used for the method is [17]:

$$[T(\omega+\Delta\omega)T^{-1}(\omega)-(1+i\tau_g\Delta\omega)I]\hat{y} = 0. \tag{4.1.1}$$

The DGD is then obtained by the relation [17], where $\rho_{1/2}$ are the complex eigenvalues of equation (4.1.1):

$$\Delta\tau = |\tau_{g1}-\tau_{g2}| = \left|\frac{\mathrm{Arg}(\rho_1/\rho_2)}{\Delta\omega}\right|. \tag{4.1.2}$$

The JME technique thus provides estimates of the DGD at samples of wavelength for a component at a particular instance in time. In a fibre with low mode coupling, such as a short concatenation of two or three high-birefringent fibres (also known as polarization maintaining fibres - PMF), the DGD will have a periodic nature over wavelength, or remain constant in the case of a single length of PMF. In long fibres, the DGD will vary in a random nature as described in Chapter 3. Since the DGD in long fibres has a Maxwellian distribution, and since samples acquired over wavelength are expected to be equivalent to samples taken over time [12], a mixture of wavelength and time samples can be used to compute a mean ($\overline{\Delta\tau}$) or root-mean-square (RMS) DGD ($\sqrt{\overline{\Delta\tau^2}}$). Either parameter is useful, and generally the two are very similar in value, as seen in Equation (3.2.4). The JME measures instantaneous DGD, and thus the mean can be directly calculated by averaging

over wavelength. Other techniques directly evaluate the RMS DGD, which is 1.085 times larger than the mean.

4.1.2 Experimental Setup

The equipment required to use the JME includes a tunable laser source, and a polarimeter, which is required to measure device output polarization. Figure 4.1 illustrates a typical measurement setup. The laser is swept in incremental steps over a wavelength range, and measurements of the output polarization for three linearly polarized input beams are made at each step, through the use of fixed polarizers at the transmission end.

Figure 4.1 JME Equipment Setup

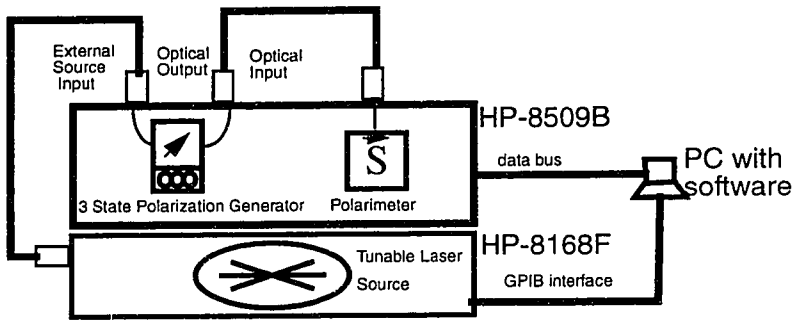

The wavelength increment during measurements must be appropriately chosen. The JME calculations cannot evaluate the exact frequency derivative of the Jones matrix, but instead estimate the frequency derivative as:

$$\frac{\partial T}{\partial \omega} = T'(\omega) \approx \frac{T(\omega + \Delta\omega) - T(\omega)}{\Delta\omega}. \qquad (4.1.3)$$

This approximation is valid provided that the differential attenuation over $\Delta\omega$ (wavelength dependent fibre loss) is negligible with respect to the total fibre attenuation [17]. This is the case for standard fibre in the 1550 nm vicinity ([30], pp. 296-298), where fibre attenu-

ation is at a minimum. Furthermore, the use of the phase difference between eigenvalues depends on the ability to approximate the eigenvalues by a complex exponential, which requires that [17]:

$$\Delta\tau\Delta\omega < \pi, \tag{4.1.4}$$

which, around 1550 nm, is equivalent to [28]:

$$\Delta\tau\Delta\lambda < 4.0[\text{ps} \cdot \text{nm}]. \tag{4.1.5}$$

Using the notion that the DGD is a stochastic function of wavelength with an autocorrelation function having a full-width at half-maximum of approximately 6 ps.nm, it would be preferable to sample the DGD at four or eight times this frequency:

$$\Delta\tau\Delta\lambda < 0.75[\text{ps} \cdot \text{nm}]. \tag{4.1.6}$$

The accuracy on the DGD is related to the accuracy with which the Jones matrix at each wavelength can be evaluated, which depends on the polarimeter used to this effect. Assuming that source wavelength error and polarization dependence of the input SOPs[1] are negligible, if the angle between unit vectors is measured by the polarimeter with error ε, then the temporal accuracy on the measured DGD is no more than $|\varepsilon/\Delta\omega|$ in magnitude [17].

Since the DGD is a statistical quantity, and since JME only scans over a finite portion of the frequency spectrum, there will always be a statistical uncertainty associated

1. Polarization dependence of the input SOPs is the dependency of the optical power on the linear input polarizers. If the light source has a null component along any of the three input linear polarizers, the polarimeter will be unable to determine the corresponding output SOP, which will affect the computation of the transmission matrix. This can be remedied by circularly polarizing the output of the light source at the input to the linear polarizers. Nevertheless, the Jones matrix algorithm is tolerant to discrepancies in power between the three measured output SOPs, as long as their intensity is within the power range specified by the polarimeter.

with the estimate of the mean DGD provided by measurement. Gisin [12] estimates the variance on the means of all measurement techniques to be:

$$\frac{\sigma_{\overline{\Delta\tau}}}{\overline{\Delta\tau}} \approx \frac{0.9}{\sqrt{\overline{\Delta\tau} \cdot \Delta\omega}}. \tag{4.1.7}$$

The wavelength range of the JME test-set depends on the operational wavelength range of the optical source, and the transmission medium bandwidth. The larger this intersection is, the more DGD samples can be acquired, which reduces the uncertainty on the mean DGD averaged over wavelength measurements. The mean DGD range of the test set depends on the granularity of the optical source: it must be able to achieve the wavelength steps required to satisfy (4.1.6).

4.1.3 Typical Results

A typical scan of the measured DGD sampled over wavelength is presented in Figure 4.2. This example is in fact not produced from real measurements, but from numerical simulations of a highly mode-coupled fibre with 1000 birefringent sections, with average section differential delays of approximately $\sqrt{\frac{1}{1000}} \cdot 2 \text{ ps} = 63 \text{ fs}$. Numerical simulations are based on the physical model described in Section 2.1, and will be further discussed in Chapter 5.

Figure 4.2 JME Scan of a Simulated Fibre (~2 ps Mean DGD)

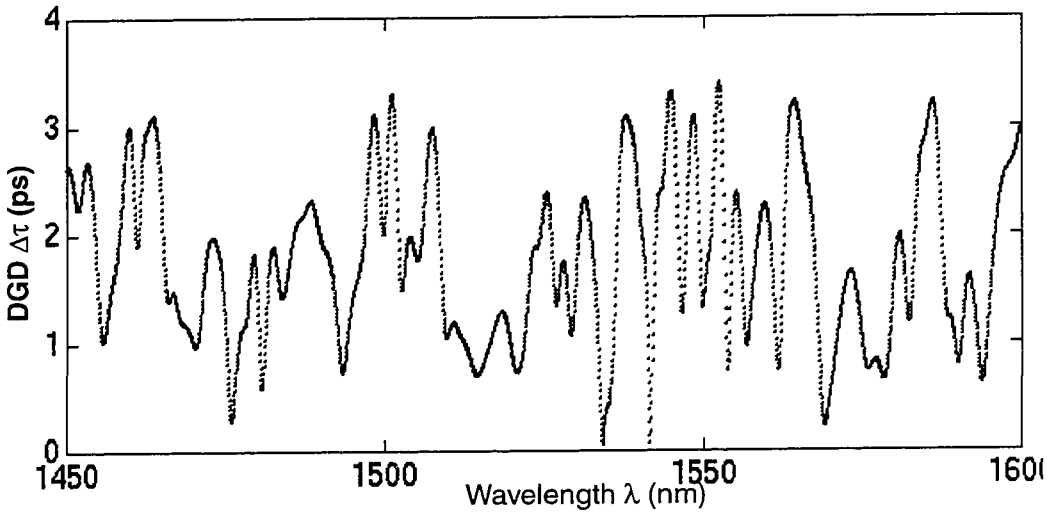

4.2 Wavelength Scanning

4.2.1 Theory

PMD is a frequency dependent phenomenon, and the frequency dependence will manifest itself in the variation of the PSPs as well as that of the DGDs. A simple technique to measure PMD involves transmitting a light-wave at a fixed polarization state through the medium and measuring the intensity of the beam at a fixed output polarization state. The fixed input polarization state can be achieved by using a polarizer, a filter which only passes the linearly polarized component of input light aligned along the orientation of the polarizer. At the output, analyzing only the polarization component parallel to a fixed output polarization state can also be done with a polarizer, which is called "analyzer" in this role.

Repeating this procedure over a range of wavelengths provides a transmission spectrum as in Figure 4.4. The mean DGD $\overline{\Delta\tau}$ of a fibre in the long length regime is related to the number of mean-level crossings N_m or number of extrema N_e by [23]:

$$\overline{\Delta\tau} \cong 4.0\frac{\langle N_m \rangle}{\Delta\omega} \text{ , and } \overline{\Delta\tau} \cong 0.824\pi\frac{\langle N_e \rangle}{\Delta\omega} \text{ .} \qquad (4.2.1)$$

For short fibre lengths (with low mode coupling), the transmission spectrum is periodic, to the extent that single lengths of PMF have sinusoidal transmission spectra. Fibre lengths in the long regime have transmission spectra with random variations.

4.2.2 Experimental Setup

The wavelength scanning technique as described in the previous section is illustrated in Figure 4.3. An alternative to using a tunable laser source is to use a light source with a large spectral width at the transmitting end, and a tunable bandpass filter at the receiving end. The filter can then be scanned over the desired wavelength range. In this scenario, the intensity of the light source and the frequency response of the tunable bandpass filter over the entire wavelength range have to be known and compensated for before analyzing the transmission spectrum.

Figure 4.3 Wavelength Scanning Setup

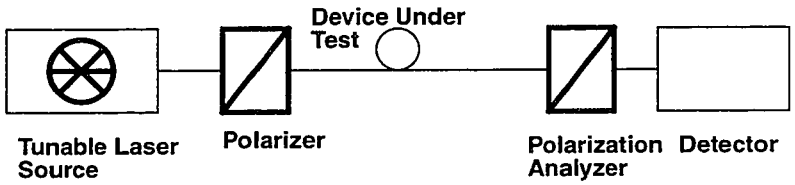

In either setup, the source spectral width or the bandpass filter's bandwidth must be smaller than [28]:

$$\Delta\lambda_{source}[\text{nm}] < \frac{1.0}{\overline{\Delta\tau}[\text{ps}]} . \qquad (4.2.2)$$

This restriction, obtained empirically, serves to minimize the range of principal states of polarization which are being explored at any given wavelength, such that the polarization

modes over the spectral bandwidth remain constant.

Again, the transmission spectrum can be seen as a signal, and it is thus important to sample it at the correct sampling interval. From (4.2.1), the average cycle $\Delta\omega_{2\pi}$ of the spectrum, which includes on average 2 extrema, can be evaluated. Sampling of the transmission spectrum should take place at a minimum of twice the extrema occurrence interval: this gives the maximum step size to use for the measurement. Reference [28] points to a maximum step size around 1550 nm of:

$$\Delta\lambda_{step}[\text{nm}] = \frac{1.625[\text{ps}\cdot\text{nm}]}{\overline{\Delta\tau}[\text{ps}]}. \tag{4.2.3}$$

As with the JME, the uncertainty on the estimate of the mean DGD is reduced as the wavelength range increases. This range will depend on the optical source used (or the intersection of the operational range of the tunable filter at the receiver and the effective spectrum of the broad light source).

This method does not rely on polarimetric accuracy, and thus the error associated with a particular point in the spectrum is the uncertainty in the light intensity measurement. Polarization dependent loss (PDL) will not affect the measurement if it is sufficiently small. Reference [23] suggests that the wavelength scanning measurement technique is tolerant of PDL up to values of at least 0.4 dB. Assuming the error on light-intensity measurements and the PDL to be negligible, the only remaining source of error is the uncertainty due to scanning over only a finite portion of the frequency domain. Poole [23] estimates the variance on the average means calculated in (4.2.1) to be:

$$\left.\frac{\sigma^2_{\overline{\Delta\tau}}}{\overline{\Delta\tau}^2}\right|_{\text{mean level}} \approx 0.44\cdot\frac{2\pi}{\overline{\Delta\tau}\cdot\Delta\omega}, \text{ and } \left.\frac{\sigma^2_{\overline{\Delta\tau}}}{\overline{\Delta\tau}^2}\right|_{\text{extrema}} \approx 0.21\cdot\frac{2\pi}{\overline{\Delta\tau}\cdot\Delta\omega}. \tag{4.2.4}$$

Both the above expressions show that the uncertainty decreases at fixed mean DGD when the wavelength range is increased. Conversely over a fixed wavelength range, the uncertainty on the mean DGD of low PMD devices is higher than that for high PMD devices.

4.2.3 Typical Results

A graph of the transmission spectrum versus wavelength is shown in Figure 4.4. The spectrum is not obtained from a real measurement, but from a numerical simulation of a highly mode-coupled fibre with 1000 birefringent sections of nominally identical average differential delay as in Section 4.1.3. The two expressions in (4.2.4) are evaluated and the results are displayed on the graph.

Figure 4.4 Wavelength Scan of a Simulated Fibre (~2 ps Mean DGD)

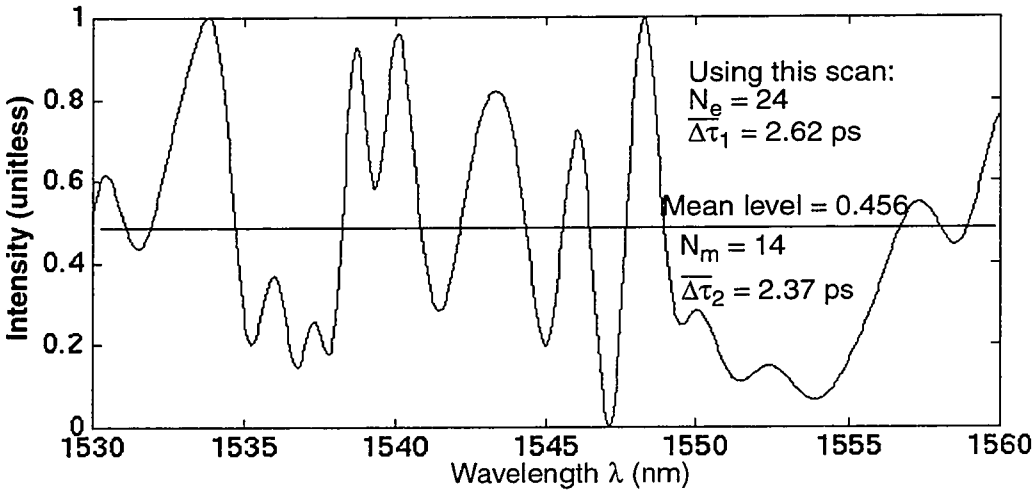

4.3 Interferometric Method

4.3.1 Theory

Interferometry is a method of measuring the autocorrelation of an optical electrical field with respect to time, using the interference pattern created when adding a waveform to a delayed copy of itself. The interferometer splits an incoming light wave along two

paths, and recombines the light at the output. The optical intensity of the recombined wave is measured while varying the spatial length of one path with respect to the other. The differential spatial length results in a time delay between the two paths, and is controlled through the movement of a mirror [13]. For a perfect monochromatic wave, the interferogram over delay resembles the coherence spectral characteristics of the source over time centred about 0. The autocorrelation peak appears when the spatial delay between the two paths is null. However, such a monochromatic wave is highly coherent, and will therefore have a large coherence time, which is reflected in the FWHM of the autocorrelation peak. A spectrally wide source with a small coherence time will have a narrow autocorrelation peak.

As mentioned earlier, PMD causes an optical wave to be split into two polarization states, adds a differential delay between the states, and recombines the two waves at the output. Therefore, at the exit of a fibre, if a polarization mode can be recombined with its orthogonal mode, and assuming the polarization modes are constant over the spectral bandwidth, the interferogram of a spectrally wide optical wave propagating through the fibre is expected to have, in addition to a central autocorrelation peak at a spatial delay of 0, two autocorrelation peaks where the magnitude of the spatial delay is equivalent to the value of the DGD. This is the principle behind the interferometric PMD measurement technique. If a source with a wide spectral width, such as a light-emitting diode (LED), is used, peaks appear at spatial delays equivalent to all of the DGDs within the spectral range of the source. In the case of a polarization maintaining fibre, the DGD is constant over wavelength, and thus a perfect PMD interferogram for this device has two predominant

peaks besides the central autocorrelation peak. More autocorrelation peaks show up in the presence of random mode coupling.

4.3.2 Experimental Setup

The interferogram is based on the phenomenon of irradiance. The intensity of the fringes of an interferogram are proportional to the dot product of the resultant electric field vector by its complex conjugate. At a given location in space, if an electrical wave has components along two orthogonal states of polarization, the dot product of one component of the field by the complex conjugate of the other is null due to the orthogonality of the vectors. To combine the electrical field in one polarization state with the field in the orthogonal mode, a method must be put into place to rotate the polarization of one path of the interferometer with respect to the other. In the setup shown in Figure 4.5, a 1/8th wave plate is used. A wave plate is an optical device made of birefringent material which has two linear axes perpendicular to the direction of propagation, namely the fast and slow axes. When an optical wave propagates through the plate, the component of the wave along the slow axis is retarded with respect to the component along the fast axis, by a phase dictated by the thickness of the wave-plate. The Jones matrix of a wave plate is:

$$T_{\text{wave plate}} = \begin{bmatrix} 1 & 0 \\ 0 & \exp(-j\Gamma) \end{bmatrix}, \tag{4.2.5}$$

where Γ is the phase (in radians) by which the slow axis is retarded over the fast axis (e.g., $\Gamma = 2\pi/8 = \pi/4$).

Figure 4.5 Interferometric Measurement Setup

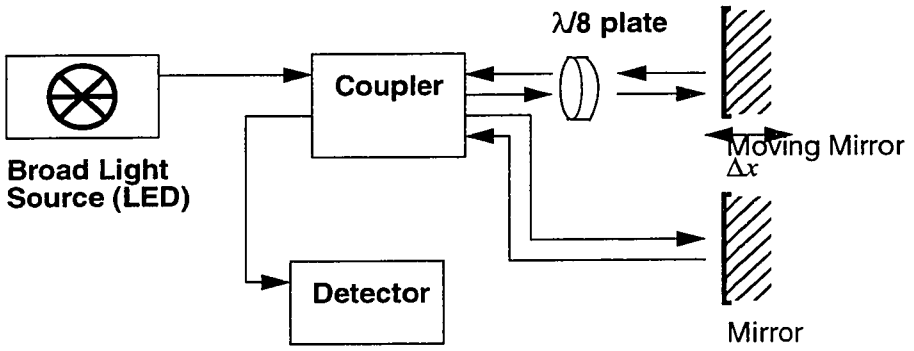

When used in conjunction with a mirror, whose Jones matrix is, ideally:

$$T_{\text{mirror}} = \begin{bmatrix} -1 & 0 \\ 0 & 1 \end{bmatrix}, \tag{4.2.6}$$

the 1/8th wave plate acts as a quarter-wave plate: a light wave propagating through the 1/8th wave plate, reflected off the mirror, and propagating through the same wave plate in the opposite direction, as described in Figure 4.5, will have effectively passed through the equivalent of a quarter-wave plate:

$$T_{\text{equiv}} = T_{\lambda/8} \cdot T_{\text{mirror}} \cdot T_{\lambda/8} = \begin{bmatrix} 1 & 0 \\ 0 & e^{-j\frac{\pi}{4}} \end{bmatrix} \cdot \begin{bmatrix} -1 & 0 \\ 0 & 1 \end{bmatrix} \cdot \begin{bmatrix} 1 & 0 \\ 0 & e^{-j\frac{\pi}{4}} \end{bmatrix} = -1 \begin{bmatrix} 1 & 0 \\ 0 & j \end{bmatrix}, \tag{4.2.7}$$

while the optical wave travelling through the other arm of the interferometer will be subject to the polarization transformation given in (4.2.6). The experimental setup shown in Figure 4.5 resembles the one used in [18].

An LED is used as the source at the input of the device under test. Linearly polarized light, making an angle of 45° with respect to the two axes of the plate, is transformed by the effective quarter-wave plate into circularly polarized light (the converse applies for incident circularly polarized light). Since circularly polarized light can be broken down

into linearly polarized components (and vice-versa), if the output PSPs of the fibre have linear (at 45°) or circular polarization states, then, as the two arms of the interferometer recombine, the delayed signal component will have a polarization component parallel to the non-delayed signal component[1]. Therefore, at a fixed wavelength, as long as both output PSPs of the fibre each have components along the two axes of the interferometer's wave plate, and as long as the light source has components along the two PSPs, the optical source component along the fast PSP can be partially recombined with the delayed component along the other PSP, and the DGD at that wavelength will correspond to a set of peaks in the interferogram. Fortunately, in highly mode-coupled fibres, the wide spectrum of the LED will explore a wide range of PSPs, such that the interferogram will contain several peaks corresponding to various DGDs. This reduces the necessity to monitor launch conditions of the optical source into the fibre.

The envelope of the resulting interferogram resembles a Gaussian. The half-width of this Gaussian can be shown to be related to the mean of the square DGD [13]. As mentioned, if the source is spectrally wide, then a multitude of DGDs will be explored by the interferometer over the frequency range of the source. The resulting interferogram will have the expected central peak superimposed upon a Gaussian representing the various DGDs [13]. The mean DGD of a highly mode coupled fibre is measured by calculating the second moment of the Gaussian after removal of the central peak.

Due to the limited spectrum of the LED, the uncertainty in the estimate of the mean DGD is identical to that calculated using other methods. It is only necessary to sub-

1. If the output PSPs at a particular wavelength are linear and parallel to the axes of the wave-plate inside the interferometer, the components of the optical source along the two PSPs cannot be recombined.

stitute the spectral width of the source for the wavelength range used with the JME or wavelength scanning methods. In addition, interferometric measurements contain additive noise and random amplitude as explained in [18], which must be compensated for. The central autocorrelation peak must also be eliminated.

In the setup described above, assuming nominally equal branch distances in each arm of the interferometer, such that the waves propagating down the two branches are subject to approximately the same attenuation, the mirror displacement Δx is related to the delay τ by:

$$\tau = 2\frac{\Delta x}{c}. \tag{4.3.1}$$

Therefore, in order to measure DGDs above τ ps, the mirror displacement Δx must be capable of exceeding $c\tau/2$, where c is the speed of light in air.

4.3.3 Typical Results

The equipment needed to perform an interferometric measurement was not available for the measurements performed in this thesis. The interferogram has an analogous equivalent to the Fourier transform of the transmission spectra of the wavelength scanning method. The main difference is the absence of the central peak corresponding to the autocorrelation of the unperturbed source. The LED source used with the interferometric method has a wide spectral width, while the source used with the wavelength scanning technique is spectrally narrow, and will have an approximately constant autocorrelation value over the time scale of interest (i.e. no central peak). The wavelength scan shown in Figure 4.4 actually extended from 1450 to 1600 nm, and its Fourier transform is shown below in Figure 4.6:

Figure 4.6 Fourier Transform of Transmission Spectrum of a Simulated Fibre

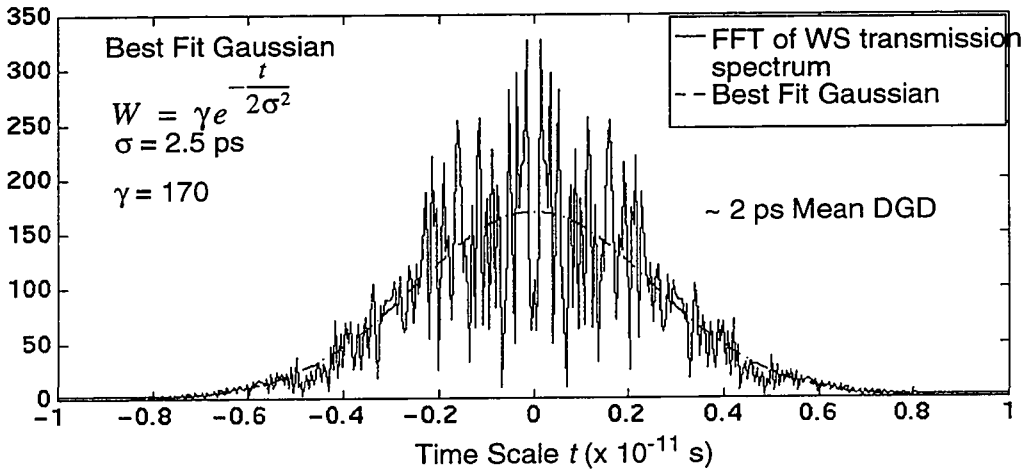

4.4 Selected Method

All of the described methods will provide estimates of the mean DGD of a device. Furthermore, the level of random mode coupling, a function of the fibre length's regime (either short or long), can be seen using any of the three methods. A DGD wavelength scan, as obtained via JME, has clear periodic components for fibres in the short length regime, and becomes random for longer devices. The same applies to the wavelength scanning technique. The interferometric technique has a few clear peaks for low mode-coupled fibres, and a Gaussian envelope for highly mode-coupled ones. Only the JME method provides an obvious way of determining the distribution of DGD, since it measures a population of samples whose distribution can be directly compared to a Maxwellian distribution.

In this thesis, there is a requirement to cross-correlate the DGD characteristics of the device at different instances in its history, so as to characterize the variation of PMD over time, or to determine whether the PMD in the device during one measurement is correlated with the PMD in the device at another measurement. This requirement eliminates

the interferometric technique. The noisy nature of interferograms makes it difficult to extract the correlation between two measurement instances. On the other hand, the cross-correlation of DGD scans and of wavelength scanning transmission spectra is straight-forward.

The fact that the JME method produces estimates of the DGD characteristic over wavelength, including instantaneous DGD samples, is the reason for its selection as the measurement technique for this experiment. For brevity, the term "JME scan" will be used to indicate the DGD samples collected during a measurement over a given wavelength range.

4.5 Accuracy and Measurement Error

From Section 3.4, it is reasonable to assume that the DGD is a stationary process over wavelength: the mean is fixed. Nevertheless, as mentioned, the finite sampling of the process conducted in the frequency window of any of the three methods discussed is inherently accompanied by an uncertainty. The uncertainty of the estimate of the mean DGD (averaged over wavelength) provided by the various PMD measurement techniques was discussed earlier in the chapter. Figure 4.7 shows the uncertainty, measured as the standard deviation of various estimates of the mean, as a function of the reciprocal window size. The reciprocal window size is defined as the inverse of the product of the mean DGD by the frequency range over which it was measured, and is a useful parameter in describing PMD since the mean DGD and the frequency domain are so closely linked. The graphs show various approximations of the uncertainty.

Figure 4.7 Uncertainty of the Estimate of the Mean

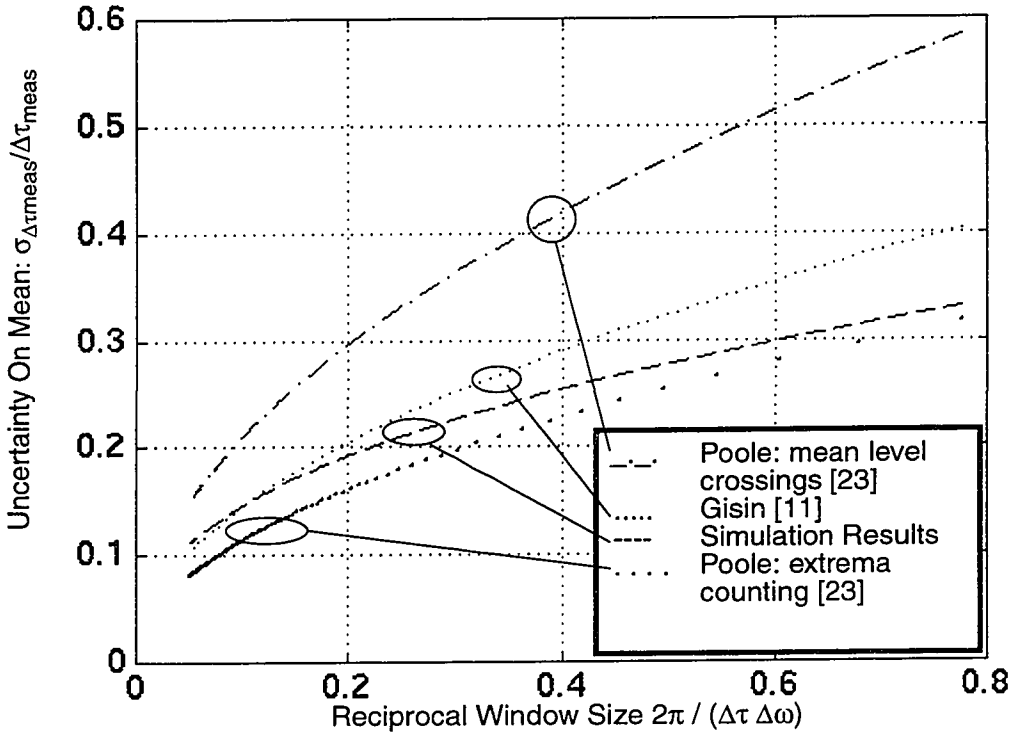

A fourth function shown on the graph is the best fit to the uncertainty of the mean DGD (averaged over wavelength) obtained from numerical simulations, as will be described in the section pertaining to simulation results.

Although the above method characterizes the variance of the estimate of the mean DGD based on the reciprocal window size, a different approach is used to evaluate the uncertainty of the JME measurement technique by estimating confidence intervals of the estimated mean DGD based on numbers of samples.

4.6 Characterizing a Device

Characterizing a device with respect to PMD means measuring the average DGD, and determining the degree of mode coupling. No mode coupling exists within a PMF,

although it does have a relatively high mean DGD which will not vary over frequency or time (DGD is constant). For such a device, it is straightforward to measure the mean DGD with a high degree of certainty. On the other hand, a long span of single mode fibre will have high mode coupling and some unknown mean DGD. In this case, we must determine how many samples are required to establish with a given precision the mean DGD.

4.7 Confidence Interval

When dealing with large populations, the confidence interval on the mean can be calculated based on methods which assume normal distributions ([20], pp. 1222-1231). For a confidence level of β, $0 \leq \beta \leq 1$, the confidence interval of the estimated mean is given by:

$$k = \frac{c\sigma}{\sqrt{n}}, \tag{4.7.1}$$

where c is defined such that:

$$\int_{-c}^{c} \frac{1}{2\pi} e^{-\frac{x^2}{2}} dx = \beta. \tag{4.7.1}$$

The interval is defined by $\hat{\mu} - k \leq \mu \leq \hat{\mu} + k$. For Maxwellian distributions, the standard deviation is given from the mean as in (3.5.1). In this case, k becomes:

$$k = c\mu\sqrt{\frac{3\pi - 8}{8n}}, \tag{4.7.2}$$

or, for a relative confidence interval, $k = \alpha\mu$, where:

$$\alpha = c\sqrt{\frac{3\pi - 8}{8n}}. \tag{4.7.3}$$

For $\beta = 95\%$, we have $c = 1.960$, such that α becomes:

$$\alpha = \frac{0.827}{\sqrt{n}}. \tag{4.7.4}$$

The number of samples can then be determined by the desired relative confidence interval. Note that for an α of 5%, $n = 274$, which means that 274 independent DGD samples must be obtained for a device to determine, at the 95% confidence level, that the mean DGD is known within +/- 5%.

4.8 Real-World Validity Test

As stated in Section 3.4, we assume that the birefringence in each section of the physical model does not change with time. In a fibre plant, temperature variation may tend to redistribute the stress / strain on constituent fibre sections of a link, however the birefringence of the link is expected to remain unchanged in the model. On the other hand, the mode coupling angle of each section with respect to the next will change. While the orientations of the sections change, the angles between sections remain uncorrelated, and the differential delays in the sections stay fixed. From the development explained in Section 3.2 in conjunction with the assumption of constant section delays, the DGD of an optical fibre is expected to be stationary in frequency and in time (over limited periods), and to be an ergodic process with respect to time and frequency averages. The significance of the assertion of stationarity is that the mean DGD of an optical fibre (averaged over frequency) will not change with time, given stable environmental conditions. Due to the limited number of samples in a JME scan, the sample mean from each JME scan will likely differ from the actual mean.

The experiment designed for this thesis attempts to mimic a real-world optical communications link. In the real world, the PMD in a fibre constantly evolves into new,

uncorrelated instances with the aid of environmental changes. In the laboratory, this evolution is generated artificially in order to obtain enough instances to provide the required number of samples in a practical time-frame. Furthermore, the SMF spans in the experiment are not subject to the same physical environment as optical cables in a typical terrestrial fibre plant: instead, the spans consist of bare fibre tightly wound around plastic spools.

In the experiment, the artificial PMD evolution over time is performed by changing the temperature of the optical fibre components. Initial measurements on the fibre spans showed that the mean DGD has a strong dependency on temperature[1]. Ruling out coincidence, in the model, this result suggested increases in the section differential delays with temperature. Such occurrences are assumed to be "non real-world events" and shall be termed thus.

Since estimates of the mean DGD are also expected to fluctuate due to the stochastic nature of the DGD process, it is important to differentiate between the statistical variation and the variation due to temperature. Therefore, it is useful to quantify the expected variation in the mean due solely to the random process.

In a JME scan, the relationship between the mean DGD, the wavelength range over which the DGD was averaged, and the variance of the mean is known (Sections 4.1.2, 4.2.2, and 4.5). Based on this relationship, a test can be designed to evaluate the probability level of any mean DGD measurement, given knowledge of the actual mean. Mean DGD measurements which fall below a chosen threshold probability level can be dis-

1. It is noteworthy that the mean DGD of the fibre spools are not dependent on the temperature history, only on the current temperature. After temperature excursions, the DGD will return to former values when the temperature returns.

carded as manifestations of "non real-world events", as defined above, although there is a possibility that they are valid measurements whose mean DGD has a low probability.

The difference between an estimate of the mean DGD (averaged over wavelength measurements) and the actual mean DGD is assumed to have a normal distribution centred on zero and with variance equal to the variance of the mean described in Section 4.5. The metric normalizing this difference by the known variance over a given wavelength range is written as [31]:

$$z = \frac{\left|\overline{\Delta\tau}_1 - \hat{\Delta\tau}\right|}{\sqrt{\sigma^2_{\hat{\Delta\tau}}}}, \tag{4.8.1}$$

where z is an abscissa on a normal distribution plot of zero-mean and unitary standard deviation, $\overline{\Delta\tau}_1$ is the measured mean, $\hat{\Delta\tau}$ is the best estimate of the actual device's mean DGD (mean of measured means), λ is the centre-wavelength and $\Delta\lambda$ is the wavelength range of the scan. The value in the denominator is a function of $\hat{\Delta\tau}$, and is more accurate when many measurements have been taken.

When the difference between two means is normalized as in (4.8.1), the metric z is expected to be smaller than $z = 0.675$ 50% of the time. Similarly, 95% of the time, z is expected to be smaller than 1.96. The actual probability of occurrence of any value smaller than the z metric is evaluated using (4.8.2) and is tabulated in many statistical references.

$$p(\Delta\tau_1 \in \text{Non-Stationary}) = \text{erf}\left(\frac{z}{\sqrt{2}}\right). \tag{4.8.2}$$

In this verification, the 95% probability is used as a threshold to determine whether a particular measurement occurred during non real-world conditions. Any measurements yielding $z > 1.96$ are discarded from the analysis.

4.9 Goodness of Fit Test

Generally, a distribution of samples of a statistical process can be examined by plotting a histogram. A χ^2 goodness of fit test can then be used as a test of conformity of a sample distribution to a theoretical distribution using the sum ([20], pp. 1232-1258):

$$\chi_0^2 = \sum_{j=1}^{K} \frac{(b_j - e_j)^2}{e_j}. \tag{4.9.1}$$

In this expression, b_j is the number of samples in the j-th interval of the distribution histogram, while e_j is the theoretical number of samples based on the probability density function and the total number of samples. The sum of the error over all bins, χ_0^2, is then a useful parameter in evaluating the goodness of the fit. For various populations of a statistical process with any given distribution, the various χ_0^2 have a χ^2 distribution with $K - r - 1$ degrees of freedom, where K is the number of bins, and r is the number of estimated parameters in the theoretical distribution. In particular, the Maxwellian distribution requires only one parameter to be estimated: the mean, μ. Thus, the χ^2 distribution of χ_0^2 values of Maxwellian populations will have $K - 2$ degrees of freedom.

Given a particular Maxwellian random process, various populations of equal size will have a distribution of χ_0^2 values ranging from 0 to positive infinity. If a χ_0^2 threshold is chosen sufficiently high in this range (above the mean of the χ^2 distribution, for example), it can be used to filter out low probability populations.

If instead a random process has an unknown distribution, let us hypothesize that a population of samples from this process has a Maxwellian distribution. A threshold is chosen as indicated above. A Type I error is committed when the population is rejected

although it does have a Maxwellian distribution. If, however, the hypothesis is not rejected although its distribution is not Maxwellian, a Type II error is being made.

One cannot quantify the probability of Type II error for a goodness of fit test, due to the infinite number of theoretical distributions that can describe a random process. But one can limit the probability of occurrence of Type I error, which is called the significance level. A significance level of 5% means that 5% of Maxwellian sample sets will be rejected as Maxwellian distributed, while 95% will not be rejected. Again, the probability that non-Maxwellian sample sets will be not be rejected is unknown.

The threshold T to choose for a particular significance level α and χ^2 distribution is tabulated, and is defined as follows:

$$\int_0^T \chi^2(x, K-r-1)dx \;=\; 1-\alpha\,. \tag{4.9.2}$$

In this thesis, we hypothesize, as suggested above, that populations of DGD samples are Maxwellian-distributed. The significance level we use is 5%, a standard value chosen for such tests. Another recommended practice maintained in this thesis is to ensure a minimum of 5 samples in each bin [20], while a minimum of 10 bins is used for all populations.

Chapter 5: Numerical Simulation Results

In this chapter, the numerical PMD simulations conducted in the thesis are described. We indicate the model that the simulations are based upon, and specify the input parameters used by the numerical simulation. The χ^2 goodness of fit test is performed on simulation results to determine how many sections are required to provide Maxwellian statistics. An expression relating the correlation bandwidth of the DGD stochastic process to the mean DGD is then obtained from PMD simulation results. To evaluate the intrinsic uncertainty in measurements of DGD, PMD simulations of a given fibre at different instances in time are used to derive expressions for (a) the variance in the estimate of the cross-correlation between JME scans and (b) the variance in the estimate of the mean DGD, averaged over wavelength. Finally, a simulation of the cascaded link system measured in the subsequent experiment is executed, to determine how to vary the PMD instances of the components, and to verify the cascaded link rule.

5.1 Numerical Simulation Description

The physical model previously described in Section 2.1 is illustrated below in Figure 5.1, and is converted into Jones matrix format in (5.1.1). We assume a set of uncorrelated section differential delays, and a set of uncorrelated mode coupling delays, such that the PMD in adjacent sections is uncorrelated. This assumption is simulated by independently generating random sequences of section differential delays and random sequences of mode coupling angle for any fibre.

Figure 5.1 SMF Physical Model

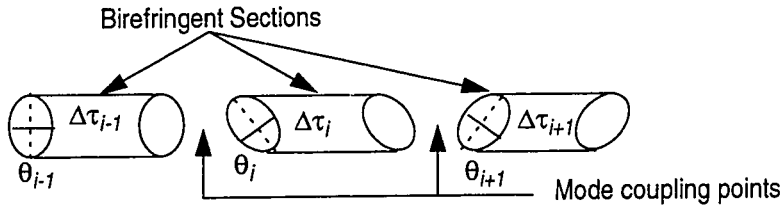

$$T_i = \begin{bmatrix} \cos\theta_i & \sin\theta_i \\ -\sin\theta_i & \cos\theta_i \end{bmatrix} \cdot \begin{bmatrix} e^{j\cdot\frac{2\pi\cdot\Delta\tau_i/2\cdot c}{\lambda}} & 0 \\ 0 & e^{-j\cdot\frac{2\pi\cdot\Delta\tau_i/2\cdot c}{\lambda}} \end{bmatrix} \cdot \begin{bmatrix} \cos\theta_i & -\sin\theta_i \\ \sin\theta_i & \cos\theta_i \end{bmatrix}. \quad (5.1.1)$$

The parameters of the simulation are: (a) number of sections N and (b) desired mean DGD $\overline{\Delta\tau}_{\text{Desired mean DGD}}$. The differential delay of the birefringent sections is chosen from a normal distribution with non-zero mean equal to $\overline{\Delta\tau}_{\text{section}}$, and with a fixed standard-deviation-to-mean ratio of $\eta = 20\%$. This ratio of 20% guarantees that for a population of approximately 100 samples from a perfect Gaussian random number generator (used to generate 100 sections delays), fewer than 1 sample will have a section delay less than 0 ps, on average, thus eliminating the requirement to manually truncate the distribution, while maintaining a reasonably large variance. From (3.3.10) and (3.4.4), and assuming that the simulated fibre is long enough such that its DGD will have a Maxwellian distribution and expression (3.2.4) will apply, the mean section DGD value is then computed by evaluating:

$$\overline{\Delta\tau}_{\text{section}} = \sqrt{\frac{3\pi}{8N(1+\eta^2)}}\,\overline{\Delta\tau}_{\text{Desired mean DGD}} \approx \frac{1.06}{\sqrt{N}}\,\overline{\Delta\tau}_{\text{Desired mean DGD}}. \quad (5.1.2)$$

Mode coupling angles are chosen for each section from a random variable with uniform distribution over $[0, 2\pi)$ which represents the angle of tilt of each section with respect to horizontal (x-axis) linear polarization. The DGD is then evaluated for wave-

lengths between 1450 and 1600 nm distanced 0.05 nm apart using the Jones matrix eigen-analysis technique. The greater the number of sections, the more the DGD statistics over frequency resemble those of a Maxwellian distribution. The simulations conducted in this thesis show that a number of sections in the order of 100 produce reasonable statistics.

5.2 Goodness of Fit to Maxwellian Distributions

The goodness of fit test is performed on results of the PMD simulator to determine how many sections are required to provide Maxwellian statistics. The tests described in Section 4.9 were conducted for this purpose.

Simulations of fibres of nominally identical mean DGD, with between 10 and 5000 birefringent sections, were performed. For each simulation, multiple JME scans with constant birefringent sections but uncorrelated mode coupling angles are produced. Independent samples are extracted from each JME scan, and the error χ_0^2 is evaluated against the theoretical Maxwellian distribution. In each case, the error χ_0^2 is minimized with respect to the selection of the theoretical distribution mean μ. Also, the ratio of standard-deviation-to-mean of DGD samples is calculated and compared to the theoretical ratio of 0.422, for an added characterization of the generated distribution.

Figure 5.2 Maxwellian Conformance Based on Number of Sections

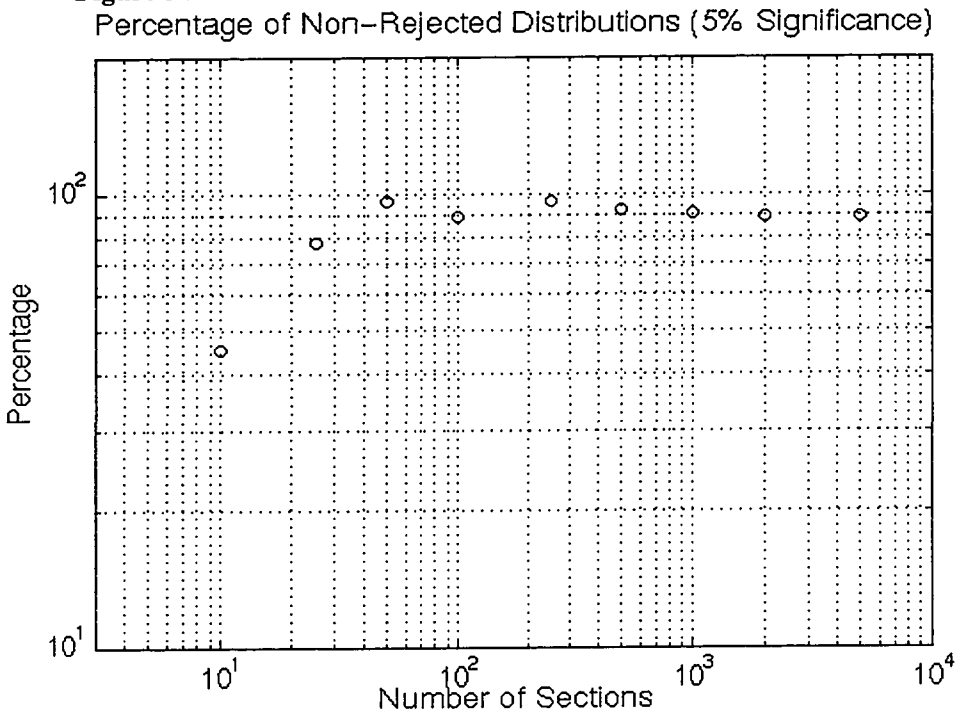

As the number of sections increases, the frequency of χ_0^2 errors below the significance threshold increases, and stabilizes as the number of sections reaches 100. At 100 sections, the standard-deviation-to-mean ratio is within 0.5% of the theoretical value of 0.422 (worst case is 42.39%). The numerical simulations appear to generate good Maxwellian statistics for fibres with more than 100 birefringent sections.

5.3 Correlation Bandwidth Constant

The autocovariance function is defined using an integral of the instantaneous DGD over an infinite wavelength range:

$$C_\lambda(\Delta\lambda) = \frac{\int_0^\infty (\Delta\tau(\lambda) - \overline{\Delta\tau})(\Delta\tau(\lambda+\Delta\lambda) - \overline{\Delta\tau})d\lambda}{\int_0^\infty (\Delta\tau(\lambda) - \overline{\Delta\tau})^2 d\lambda}. \qquad (5.3.1)$$

The DGD samples which are provided by the simulations and measured using the JME technique are limited to a finite wavelength range. For this reason, only an estimate of the autocovariance function can be obtained. Several techniques exist for this purpose ([21], pp. 729-754). The technique used here in estimating the autocovariance function is to: (a) obtain a sequence of N DGDs sampled over wavelength; (b) subtract, from the sequence of DGDs, its sample mean; (c) repeatedly evaluate the cross-correlation of the sequence with shifted versions of itself; (d) divide the values found in the previous step by the number of overlapping samples in the cross-correlated sequences (i.e., the factor $1/(N\text{-}i)$ in (5.3.2)). The maximum value of the estimate will correspond to the cross-correlation of the sequence by itself (and divided by N). If the DGD samples in the sequence are numbered 1 to N, the expression below describes the process mathematically:

$$\hat{C}_{\lambda}(i) = \frac{1}{N-i} \cdot \sum_{k=1}^{N-i} (\Delta\tau_k - \overline{\Delta\tau}) \cdot (\Delta\tau_{k+i} - \overline{\Delta\tau}) \;, i \in \{0, 1 \ldots N-1\}. \quad (5.3.2)$$

If the DGD samples are acquired at wavelength samples distanced $\Delta\lambda_{step}$ apart, the quantity $\hat{C}_{\lambda}(i)$ is an estimate of the autocovariance function $C_{\lambda}(\Delta\lambda)$ at $\Delta\lambda = i \cdot \Delta\lambda_{step}$.

The correlation bandwidth was obtained for fibres of different mean DGD as follows: a JME-scan is processed to yield an estimate of the autocovariance function, which in turn has a full-width at half-maximum (FWHM) around the central peak. The correlation bandwidth for a particular fibre is estimated here as the average FWHM over an ensemble of uncorrelated JME scans of the fibre. Uncorrelated JME scans of a same fibre were simulated by assuming that uncorrelated scans or instances of PMD in a fibre occur when its set of birefringent sections remains constant, but its set of mode coupling angles varies from scan to scan. This should, according to (3.3.10), maintain the same mean DGD

(averaged over wavelength) over the uncorrelated JME scans, provided there is a large number of sections in the fibre. This process is repeated for 7 fibres of different mean DGD, while the correlation bandwidth at each DGD is averaged over 100 uncorrelated JME scans. Around 1525 nm, the bandwidth is found to be related to the mean DGD as follows (3.5.4):

$$\Delta\lambda_c\overline{\Delta\tau} \approx 5.8[\text{ps} \cdot \text{nm}]|_{1525\text{nm}}, \text{ or} \tag{5.4.1}$$

$$\overline{\Delta\tau} \cdot \Delta\omega_c \approx 2\pi \cdot 0.75[\text{s} \cdot \text{Hz}]. \tag{5.4.2}$$

A log-log plot of correlation bandwidths versus mean DGD, for simulations of fibres of various mean DGDs, is given in Figure 5.3, while a histogram of the correlation bandwidths obtained from 100 uncorrelated JME scans of fibres of identical set of birefringent sections, with mean DGD (averaged over wavelength and fibres) of 1 ps, is plotted in Figure 5.4.

Figure 5.3 Correlation Bandwidth vs. Mean DGD ~ 1525 nm

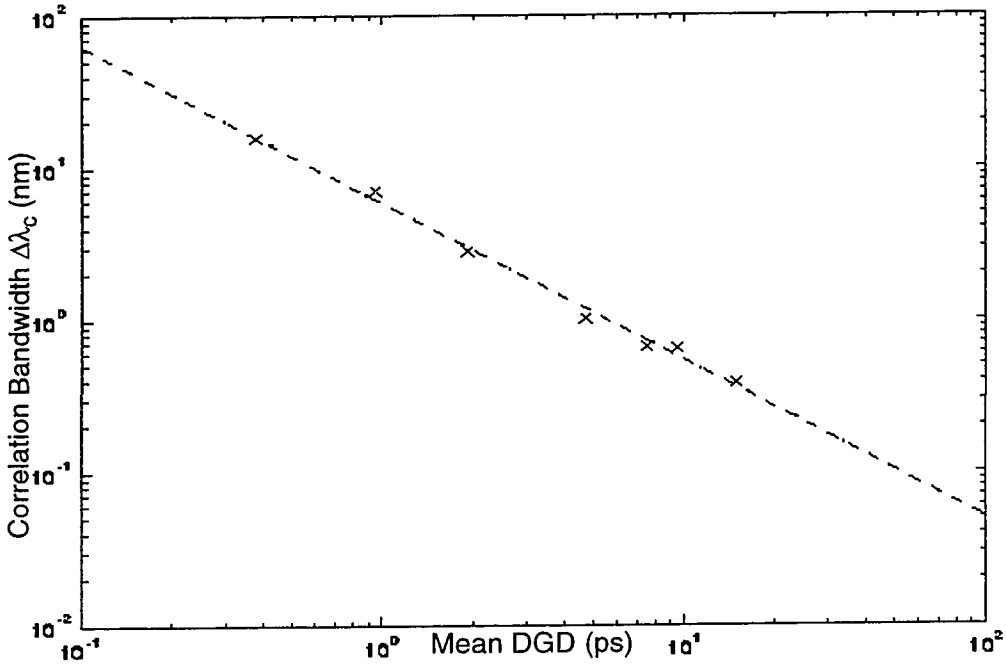

Figure 5.4 Histogram of Simulation Correlation Bandwidth ~ 1525 nm

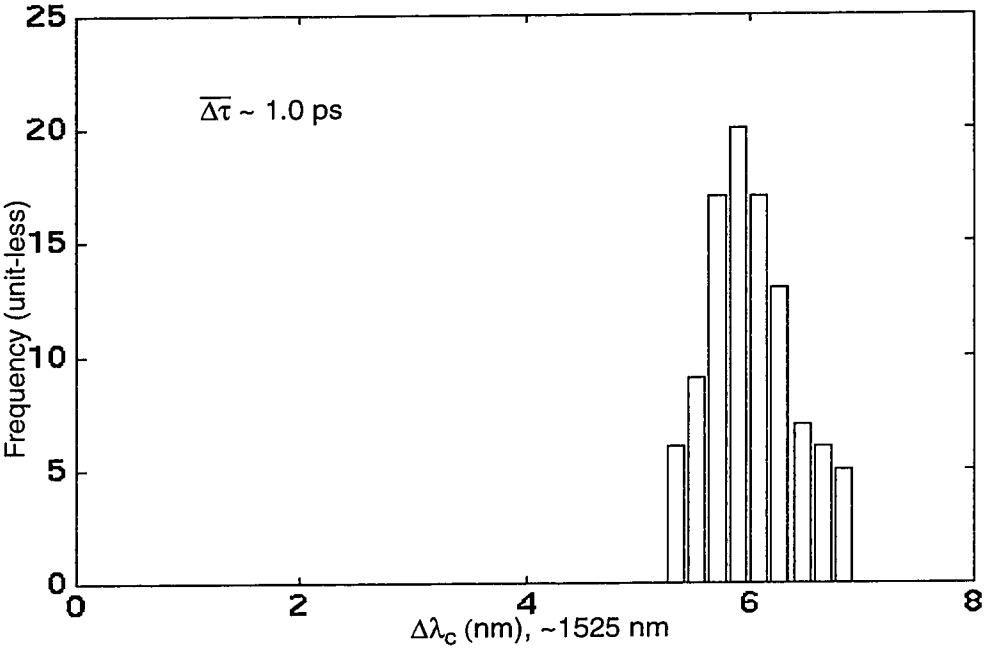

5.4 Identical Fibres of Uncorrelated Instance

As described in the simulations generated in the previous section, we define an ensemble of fibres of identical construction as an ensemble of sets of DGD samples of wavelength, where each set corresponds to a simulated physical model, using an independent set of mode-coupling angles from model to model, but a fixed set of section differential delays over the ensemble of models. Based on the assumption that the changes over time of section birefringence are negligible with respect to the changes in the mode coupling angles, we use an ensemble of fibres of identical construction to model a single fibre at different, uncorrelated (with respect to PMD) instances in its lifetime. Each simulation (which yields a single JME scan or wavelength ensemble) shall be said to represent an "instance" of the fibre.

In this section, such simulations are used to evaluate two different statistical aspects: the variance in the estimated cross-correlation of two supposedly uncorrelated instances of the fibre, and the variance in the mean DGD estimated at two uncorrelated instances of the fibre, both as a function of the wavelength range of the JME scan.

5.4.1 Variance in Cross-Correlation Estimates

The cross-correlation coefficient between the DGD characteristics of a fibre at two uncorrelated instances t_1 and t_2 can be evaluated over wavelength, and is given by:

$$\Phi(t_1, t_2) = \frac{\int_0^\infty (\Delta\tau_1(\lambda) - \overline{\Delta\tau}_1)(\Delta\tau_2(\lambda) - \overline{\Delta\tau}_2)d\lambda}{\sqrt{\int_0^\infty (\Delta\tau_1(\lambda) - \overline{\Delta\tau}_1)^2 d\lambda \cdot \int_0^\infty (\Delta\tau_2(\lambda) - \overline{\Delta\tau}_2)^2 d\lambda}}. \qquad (5.5.1)$$

The value of the coefficient between two uncorrelated instances is expected to be null, if evaluated over an infinite wavelength range. However, due to the finite wavelength range

of the JME scan, the estimate of the coefficient becomes:

$$\Phi_{1,2} = \frac{\sum_{i=1}^{N} (\Delta\tau_1(\lambda_i) - \overline{\Delta\tau}_1)(\Delta\tau_2(\lambda_i) - \overline{\Delta\tau}_2)}{\sqrt{\sum_{j=1}^{N} (\Delta\tau_1(\lambda_j) - \overline{\Delta\tau}_1)^2 \cdot \sum_{k=1}^{N} (\Delta\tau_2(\lambda_k) - \overline{\Delta\tau}_2)^2}}, \tag{5.5.2}$$

and a cross-correlation estimate determined between two uncorrelated scans is likely to differ somewhat from the expected null. This is due to the fact that the averaging is limited for a finite wavelength range, and therefore statistical fluctuations cause the measurement to deviate from the zero mean.

Using the ensembles of fibres of identical construction generated in Section 5.3, for each ensemble, the various JME scans are cross-correlated to find the mean and variance of the estimated cross-correlation coefficient. The mean is expected to be null, as stated, while the variance is expected to increase as the number of correlation bandwidths in a scan decreases. Simulation results support this statement, as seen in Figure 5.5. A best fit to the simulation data is reported in (5.6.1).

Figure 5.5 Uncertainty of Cross-Correlation Value

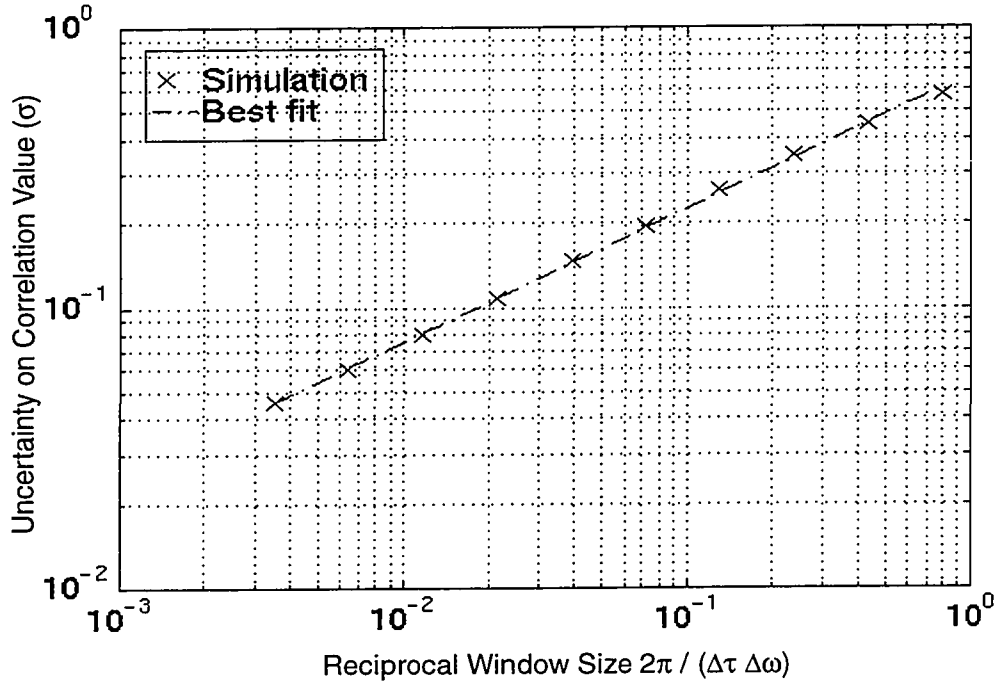

The mean cross-correlation coefficient was found to be approximately 0 for all ensembles, while the standard-deviation was found to be inversely proportional to the square-root of the product of mean-DGD and JME scan wavelength range:

$$\sigma_{correlation} \approx 0.67 \sqrt{\frac{2\pi}{\Delta\tau\Delta\omega}}. \qquad (5.6.1)$$

5.4.2 Variance in Estimates of Mean DGD

The variance in the estimate of the mean DGD from measurements is stated in Section 4.1.2. Modelling a single fibre at different instances using the ensemble of identically constructed fibres, we expect the mean DGD averaged over wavelength to be constant over the different JME scans of the ensemble. If the wavelength range of the JME scan were infinite, the mean square DGD would be equal to the root-sum-of-squares of the

individual section birefringence values as in (3.3.10). This model would attest to the ergodicity of the PMD process, with respect to averages over wavelength.

However, the JME scans are, in practice, restricted to a finite wavelength range, which will decrease the accuracy of the estimate of the mean DGD. It is reasonable then to state that measuring the mean DGD of a fibre, averaged over a given wavelength range, is likely to provide a different answer at two different times, provided that the DGD characteristics in the fibre are uncorrelated between the two instances.

From an ensemble of identically constructed fibres, we can extract a set of mean DGDs (averaged over wavelength). The standard deviation of this set of mean DGDs is expected to be equal to the uncertainty (expressed as a standard-deviation) in the mean DGD (averaged over wavelength) due to the finite wavelength range of the JME scan. This uncertainty is expected to increase as the number of correlation bandwidths in the finite wavelength range decreases (the number of correlation bandwidths in a JME scan is equivalent to the number of independent samples of the Maxwellian distribution). From the numerical simulations, the relation below is found, and is plotted in Figure 5.6 (and in Figure 4.7 for comparison with predicted curves).

$$\frac{\sigma_{\overline{\Delta\tau}_{measured}}}{\overline{\Delta\tau}_{measured}} \approx 0.35\left(\frac{2\pi}{\overline{\Delta\tau}\cdot\Delta\omega}\right)^{2/5}. \qquad (5.6.2)$$

Figure 5.6 Uncertainty Of Estimate of Mean from Simulations

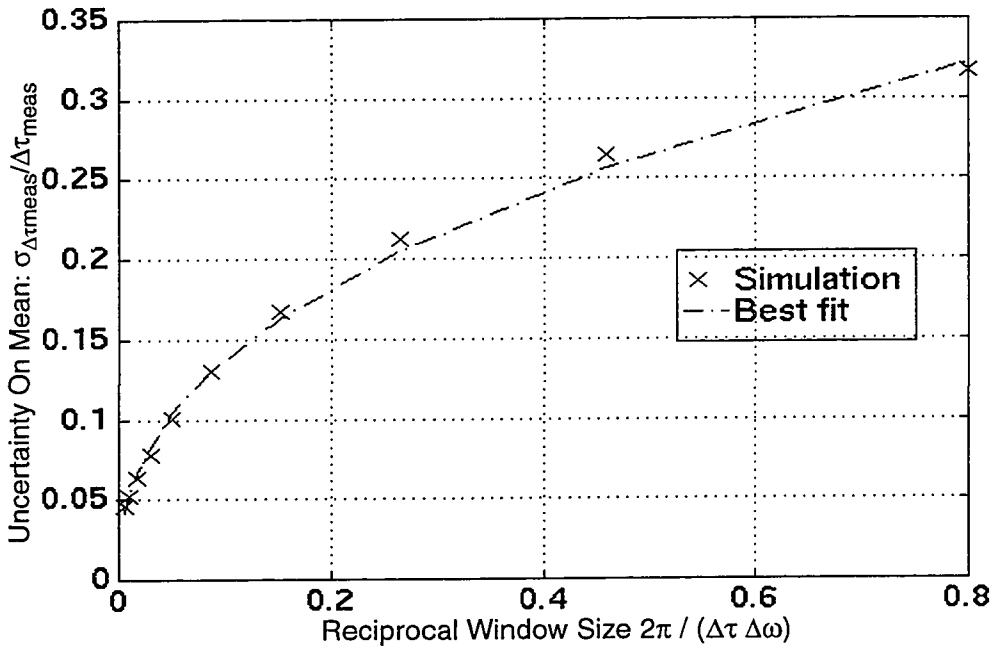

It is noteworthy that the standard-deviation curve fits closely with the approximations found in the literature (Figure 4.7). It would appear to be bounded by Poole's approximation [23] based on the extrema-counting technique when the reciprocal window is large, and by Gisin's approximation [12] when the window is small. The agreement between the results of the simulation and the approximations found in the literature would attest to the use of an ensemble of fibres of identical construction to model a fibre at uncorrelated instances in time.

5.5 System with Components of Fixed and Varying PMD

The system which this experiment is attempting to measure contains single mode fibre spans, dispersion compensating modules (DCM) and Erbium doped fibre amplifiers (EDFA). In a typical communications system, the DCMs and EDFAs are kept at controlled environmental conditions. However, the DCMs used in this experiment are the greatest

contributors of DGD. Intuitively, keeping them at constant temperature might highly correlate the DGD scans. Using uncorrelated mode-coupling angles to model the effects of temperature variations, an ensemble of numerical simulations of the system are performed with spans having (a) nominally the same DGD as the devices in the real experiment, and (b) a quantity of sections proportional to the fibre length of the real devices. However, the mode-coupling angles of the EDFAs and DCMs are kept constant over the ensemble, while those of the fibre are allowed to vary.

The simulations of the above system are shown to have a mean cross-correlation, calculated using (5.5.2), significantly higher than zero (approximately 40%), with a standard deviation of 10%. In fact, all cross-correlation coefficients are positive (see Figure 5.7). This high correlation is due to the high DGD contribution of the DCMs with fixed PMD. The conclusion to draw from this simulation is that, in order to mimic a real-world system which varies sufficiently with time to allow successive JME scans to become uncorrelated[1], the PMD of the DCMs in the experiment must be made to vary with temperature due to their high DGD contribution.

1. In such real-world systems, the fibre spans would be the main DGD contributors. Although this may not be the case in all real-world systems, only those systems whose fibre spans have high DGD are of concern in the study of PMD impairments.

Figure 5.7 Cross-Correlation Plot[1] With High DGD Contributors Fixed

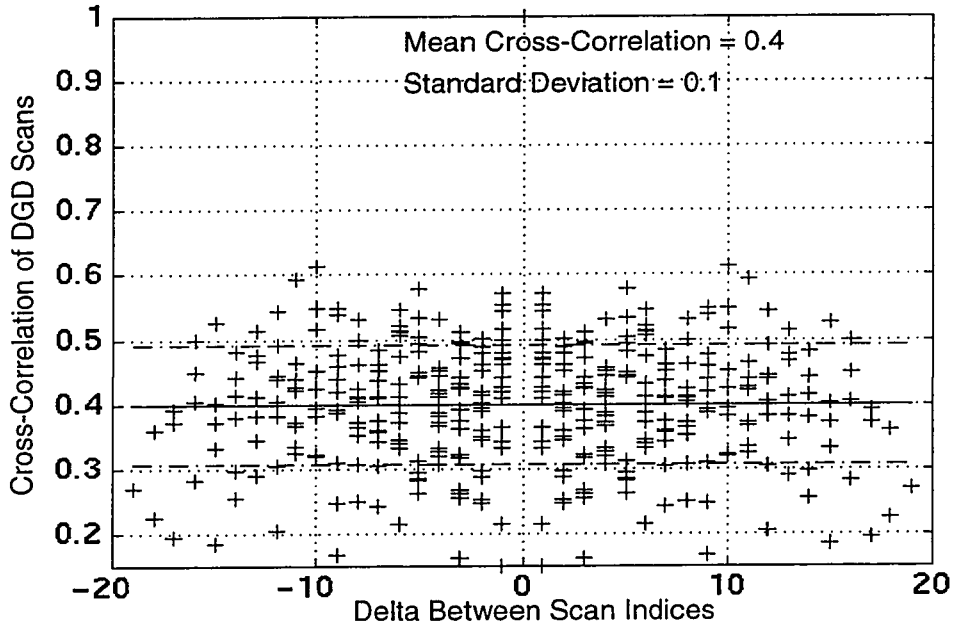

5.6 Validity of Cascaded Link Rule

The cascaded link system simulations described in Section 5.5 were considered to verify the cascaded link rule. For each "instance", the mean DGD of the cascaded link was calculated using the root-sum of squares of the mean DGDs of the components, and was compared to the mean DGD evaluated over the entire concatenated link.

The confidence intervals of each of the components and of the entire link itself were evaluated by determining the correlation bandwidth and thus the number of independent samples in each JME scan. The confidence intervals of the components, or error-bars, were added using RSS to determine the error-bar on the calculated value, while

1. The simulated DGD scans used for this graph are numbered 1-20. The horizontal axis of this graph represents the difference between the two DGD scan indices whose cross-correlation is plotted above. Several combinations have the same index-delta, and therefore more than one cross-correlation value can be plotted at a same abscissa. The graph is symmetrical about the x=0 vertical axis. Unitary cross-correlation values (on the x=0 axis) are discarded when evaluating cross-correlation mean and variance.

the confidence interval based on the JME scan of the entire link was used as the actual error bar. In all "instances" of the numerical simulations, the error-bar around the actual mean DGD overlapped the error-bar around the calculated value. This overlap supports the validity of the cascaded link rule.

5.7 Summary

The numerical simulations were largely used to produce ensembles of identically constructed fibres. The minimum number of sections needed to mimic a highly mode coupled fibre was determined. Using this number in subsequent simulations, the relation between mean DGD and correlation bandwidth was estimated, which will be compared to the values obtained from measurements. This initial relation will be used to estimate the number of uncorrelated DGD samples per wavelength scan for each optical device to be measured.

The simulations also provided agreement with the literature on the uncertainty in estimates of the mean DGD based on the measurement wavelength range. This expression can be substituted into the real-world validity test (4.8.1). Furthermore, an expression estimating the uncertainty in cross-correlation values of JME scans was obtained, which will help determine the likelihood that JME scans are uncorrelated if their cross-correlations coefficients are not null.

Finally, a simulation of the system with components of fixed and varying polarization characteristics has confirmed that large PMD contributors will highly correlate DGD scans if their polarization characteristics do not vary with time. This result will be used in the experimental portion of the thesis discussed in Chapter 6. Furthermore, the simulations suggest that the cascaded link rule is valid.

Chapter 6: Cascaded Link System Measurements

The objective of this thesis is to (a) characterize the PMD in the optical components of a digital communications system, and (b) confirm the validity, in practice, of the expression (3.3.12) linking the PMD of the system to the PMD in the components. To accomplish the latter goal in this chapter, a typical communications system is designed to identify the required components. The PMD of the components is then characterized using the Jones matrix eigen-analysis measurement technique described in Chapter 4. The PMD of the entire link is then measured, and compared with the PMD that would be predicted from the measured PMD of the constituent pieces.

6.1 System Configuration

The configuration of the optical communications link to be characterized is described in Figure 6.1. The link is a three span, amplified link, with pre- and post-amplifiers, as well as dispersion compensating modules at front and back end. Dispersion compensating modules (DCMs) are typically used as channel equalization for the chromatic dispersion which occurs along the length of the SMF spans. This configuration is a typical real-world terrestrial digital optical communications link. In practice, the Erbium-doped fibre amplifiers (EDFAs) and DCMs are kept in climate controlled shelters, while the fibre spans are in buried cables several feet under ground. The fibre spans are labelled F1, F2 and F3, while the EDFAs are numbered 1 to 4, and the DCMs 1 and 2.

Figure 6.1 Cascaded Link Configuration

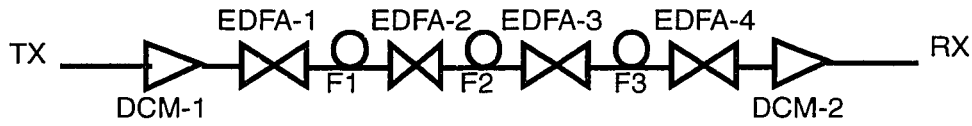

6.2 Experimental method

6.2.1 Methodology

The measurement of the DGD in the components by the JME method was explained in Section 4.1. The generation of uncorrelated instances for each device under test remains to be described.

If we first determine the temperature change (the correlation temperature) that produces uncorrelated scans of the DGD for the device, then by stepping the temperature by this amount, we produce additional uncorrelated sample measurements of the DGD. Varying the ambient temperature is the key means used in this experiment to produce uncorrelated DGD samples.

In order to validate the above approach, two assumptions have to be verified. The first assumption concerns whether the mean DGD itself of a device exhibits any temperature dependence; as explained in Section 4.8, this thesis is based upon the real-world assumption that the mean DGD (averaged over wavelength) is constant over time. Although a change in the DGD characteristics over temperature is acknowledged and depended upon to determine the correlation temperature, the mean is expected to remain constant.

The second assumption concerns the "reversibility" of a temperature change on a particular device's PMD characteristics. By "temperature-irreversible", we mean that, if the DGD characteristic is measured at some initial temperature following which the temperature is subjected to an excursion exceeding the correlation temperature and subsequently returns to the initial temperature, then the new DGD characteristic is not correlated with the initial one.

For components which exhibit temperature dependence in their mean DGD, one must choose the temperature at which one wishes to evaluate the mean DGD. If such a device is "temperature-irreversible"[1], one must then subject the temperature to excursions of magnitude equal to the correlation temperature between uncorrelated instances.

For components which do not exhibit temperature dependence in their mean DGD, changing the temperature by the correlation temperature is sufficient between measurements of DGD to generate uncorrelated instances. Furthermore, provided that the process is "temperature-irreversible", two measurements at the same temperature are permissible, as long as a temperature excursion exceeding the correlation temperature has taken place in between.

If any of the components is temperature dependent, then evidently the cascaded link system will have to be subject to similar temperature excursions as the temperature-dependent components, in order to generate new uncorrelated instances.

6.2.2 Measurement Equipment Used

The equipment used in the experiment is listed below. As described in Section 4.1, a tunable source with narrow spectral width (HP 8168F) and a polarimeter (HP 8509B) are required to perform the measurements. A PC equipped with software from the equipment manufacturer (Hewlett-Packard) synchronizes the laser with the polarimeter and performs the analysis on Jones matrices to calculate the DGD. A power meter is required to ensure continuity and fibre cleanliness throughout the fibre links.

- HP 8168F Tunable Laser Source

1. In this context, irreversible means that as an uncorrelated instance is achieved by changing the temperature, the previous uncorrelated instance cannot be re-generated by reversing the temperature change.

- HP 8509B Polarization Analyzer (includes Polarization Controller, Polarimeter)
- PC with HP software to control HP 8168F and 8509B
- EXFO Optical Power Meter
- Tenney / Watlow Oven Chamber

6.2.3 Devices Measured

The devices required to construct the digital communications link described in Section 6.1 are listed below. Three Corning SMF-28 single mode non-dispersion-shifted[1] fibre (NDSF) spans which nominally measure 80 km were used in the experiment. This type of fibre is representative of a large portion of existing fibre plants. The dispersion compensating modules are also manufactured by Corning. A 'DCM-40', labelled 'DCM-1', was inserted at the front end (closest to "transmitter", or light-source) of the system, while a 'DCM-60', labelled 'DCM-2', was used at the back end (nearest the "receiver", or polarimeter). Four EDFAs manufactured by AMOCO, Photonetics, Pirelli and Oprel respectively were used to amplify the signal before, after and between the fibre spans.

- 3 x 80 km non-dispersion shifted fibre (NDSF) spans
- 4 x EDFAs
- 2 x DCMs

1. When single mode fibres were first manufactured, they were in general non-dispersion-shifted fibres. In dispersion-shifted fibres, the silica pre-form has been doped to shift the chromatic dispersion such that its null is around 1550 nm, thus reducing impairments in digital communications in this low-loss wavelength regime.

6.2.4 Measurements

The DGD was measured using the JME technique described previously. Temperature cycling of fibre spans and DCMs was conducted in an oven chamber. All components in the oven were equidistantly located from the heating and cooling sources (Figure 6.2). The temperature of the spools and DCMs was measured with two thermo-couples. One thermo-couple was placed in the inner diameter of a sample fibre spool, which was sealed off from air circulation. The other thermo-couple was taped to the outer diameter of the same sample fibre spool. The difference in temperature readings for the two thermo-couples at steady-state operation was 0.20 C, which is insignificant with respect to the temperature excursions required to change the instance. When measuring temperature correlation, the mean temperature of any component in the oven chamber during a JME scan is taken as the average of the inner and outer thermo-couple readings of the sample fibre spool. Since the inner thermo-couple was most sheltered from heating and cooling sources, its reading changed at a slower rate than the outer thermo-couple during both heating and cooling. A temperature excursion was achieved when the inner temperature had changed by the desired excursion.

Figure 6.2 Oven Chamber Setup

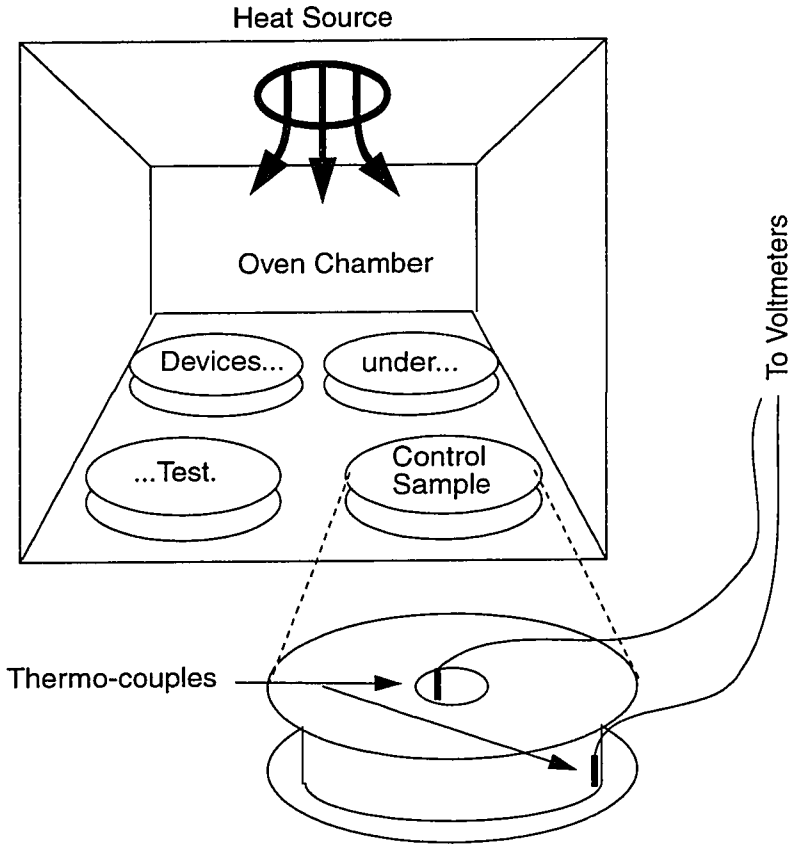

6.3 Individual Component Results

6.3.1 Correlation Temperature

The correlation temperatures were measured for the components tabulated in Table 1 (including some which do not figure in the cascaded link). They were estimated by computing the FWHM of the cross-correlation plot (6.3.1)[1], averaged over temperature (6.3.2):

1. A plot of the cross-correlation coefficients obtained with expression (6.3.1) versus the temperature difference T_1 - T_2. Since there are several such points in the vicinity of a temperature difference ΔT, these points are averaged (6.3.2), and the FWHM of the curve joining these averages is evaluated.

$$\tilde{C}_T(T_1 - T_2) = \frac{\sum_{i=0}^{N-1} (\Delta\tau(T_1, \lambda_i) - \overline{\Delta\tau})(\Delta\tau(T_2, \lambda_i) - \overline{\Delta\tau})}{\sqrt{\sum_{i=0}^{N-1} (\Delta\tau(T_1, \lambda_i) - \overline{\Delta\tau})^2 \sum_{j=0}^{N-1} (\Delta\tau(T_2, \lambda_j) - \overline{\Delta\tau})^2}}, \quad (6.3.1)$$

$$\overline{\tilde{C}_T}(\Delta T) = \frac{1}{M} \sum_{k=0}^{M-1} \tilde{C}_T(T_{l_k} - T_{m_k}), \qquad \Delta T - \delta T < |T_{l_k} - T_{m_k}| < \Delta T + \delta T. \quad (6.3.2)$$

All of the JME scans used in a cross-correlation plot were within the bounds set by the real-world validity test, such that the DGD process could be considered stationary over the temperature range considered.

Table 1 Correlation Temperatures

Component	Fibre Length	Half-Width at 0.5 Correlation (half-maximum)
Oprel EDFA	10 m	96 C
DCF	1 000 m	12 C
DCM-40	7 000 m	3.4 C
SMF	20 000 m	2.2 C
SMF	80 000 m	1.0 C

A log-log plot of the T_c half-width against fibre length is provided in Figure 6.3, and suggests that they are related. A best-fit straight line passing through the points suggests that T_c (in C) is inversely proportional to the square root of l.

Figure 6.3 Correlation Temperature vs. Length

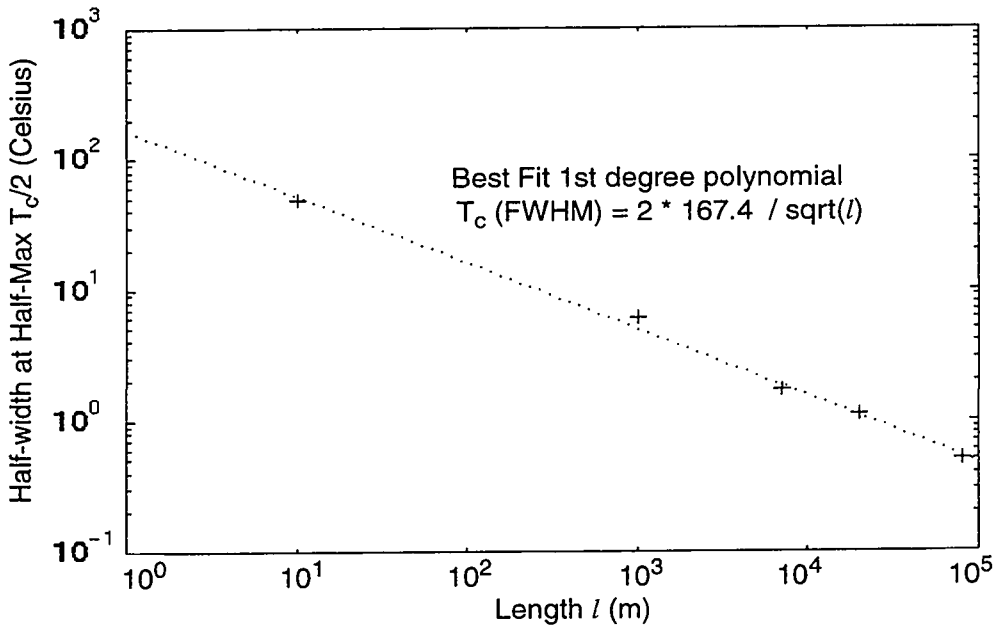

$$T_c \approx \frac{335}{\sqrt{l}}. \tag{6.3.3}$$

6.3.2 Fibres

The measured correlation temperature for 80 km SMF is 1 C. Actual measurements were conducted at least 1 C apart in average temperature, but usually in the order of 10 C. Initial measurements showed temperature dependence of the mean DGD over the 25 - 55 C range, but not below. For this reason, temperature cycling of the fibre spools was restricted to the range 0 - 23 C. The decorrelation which occurred over temperature appeared to be "temperature-irreversible", since same temperature DGD wavelength scans did not exhibit high-correlation.

Due to the observation of non real-world conformance and strongly correlated JME scans, some measurements were discarded. The non real-world conformance was

seen to happen between JME scans at different temperatures, hinting at a temperature dependence of the mean DGD over the range 0 - 23 C. Since measurements were discarded after completion of the experiment, the required number of independent samples for a 5% confidence interval on the mean was not achieved for all fibre spans. Statistical information on the acquired population of independent DGD samples is tabulated in Table 2, while DGD related data appears in Table 3.

Table 2 Fibre Span Statistical Measurement Data

Fibre span label	JME scans		Independent samples	Cross-correlation between JME scans		Maxwellian histogram		
	Total	Reject		Mean	σ	Bins	χ_0^2 fit parameter	95% Threshold
1	32	6[a]	312	4.8%	26%	15	12.3 49.8%ile[b]	22.36
2	28	5[a]+1[c] +3[d]	304	8.2%	23%	15	10.9 38.4%ile	22.36
3	27	9	162	4.3%	29%	11	6.76, 33.8%ile	16.92

a. Not all measurements were taken at 23 C. Overall measurements still showed slight temperature dependence from 0 to 23 C (mean DGD increasing with temperature), and thus only ambient temperature measurements were kept.

b. The "%ile" indicates the percentage of actual Maxwellian populations which have a χ_0^2 value smaller than or equal to the one posted.

c. One DGD scan had an improbable mean, and the measurement was considered not to be a valid real-world occurrence. This was possibly due to a thermally unstable fibre spool.

d. Three JME scans were highly correlated with other scans, and thus rejected.

Table 3 Fibre Span DGD Results

Fibre span label	Length (km)	Mean DGD (ps)		$\frac{\sigma}{\mu}$	Conf. inter-val	PMD factor $ps/\sqrt{km}$	$\Delta\lambda_c$ (nm)	Correlation bandwidth constant ~1513nm
		Sam-ple	Best fit					
1	86.646	0.434	0.440	41.4%	4.7%	0.047	12.6	5.5[a] - 0.71[b]
2	81.938	0.588	0.597	44.1%	4.7%	0.065	9.32	5.5 - 0.71
3	82.515	0.312	0.321	42.7%	6.5%	0.034	16.5	5.2 - 0.67

a. Units are nm ps.
b. Unit-less: Hz s.

The χ_0^2 results show a reasonable Maxwellian fit for all three fibre DGD distributions at the 5% significance level.

Figure 6.4 Fibre Span DGD Histograms

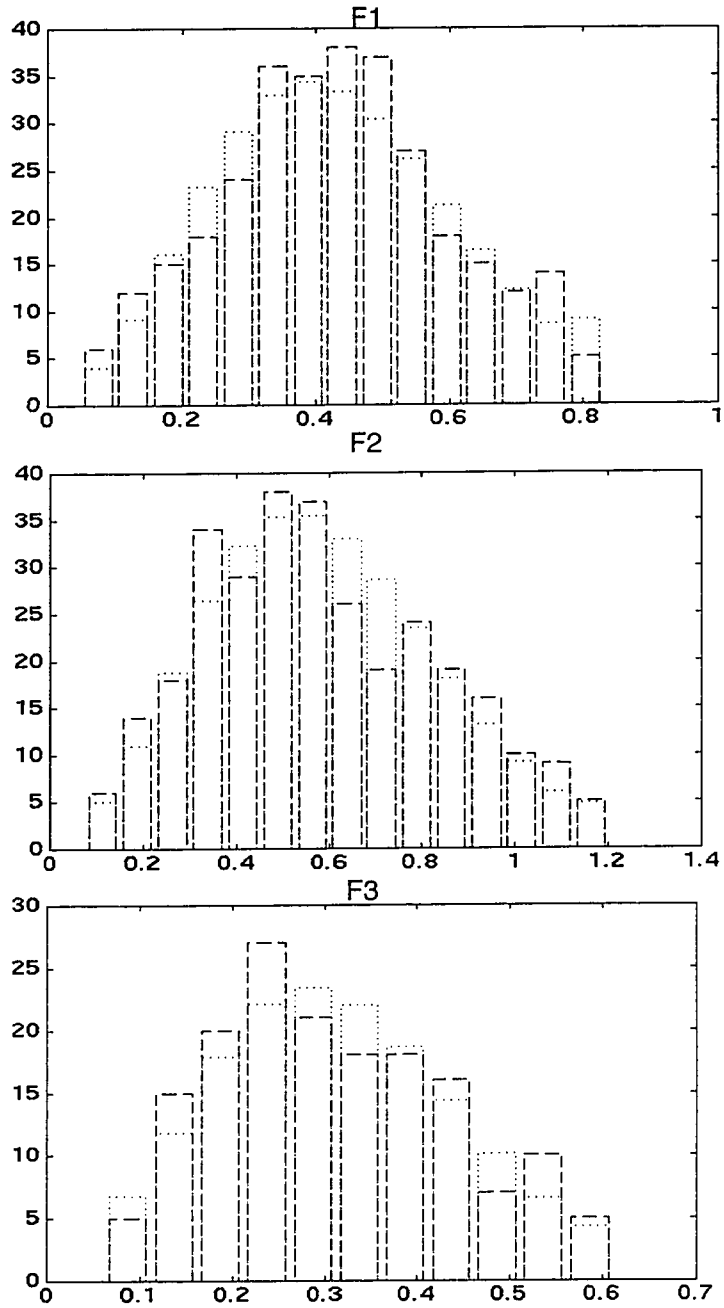

As expected, the fibre spans have long-length regime PMD distributions. The fibres used have a PMD coefficient lower than 0.07 ps/sqrt(km). The PMD coefficient over

the link comprised of the three fibre spans cascaded back-to-back is nominally 0.04 ps/sqrt(km). The average correlation bandwidth constant is 5.4 ps.nm or 0.70 s.Hz, which is close to the anticipated value of 5.8 ps.nm or 0.75 s.Hz.

6.3.3 DCMs

The two dispersion compensating modules represented the largest PMD contribution to the system. Due to the high mean DGD of the DCMs, fewer JME scans were required to generate the required number of independent samples.

DCM-1 had a correlation temperature of 3.4 C. All measurements of DCM-1 were conducted at least 5 C apart. The same excursion temperature was used for DCM-2, which is composed of a longer length of fibre, and according to (6.3.3) would have a smaller correlation temperature. Unlike the fibre spans, the mean DGDs of the DCMs were constant over the entire temperature range.

Table 4 DCM Statistical Measurement Data

DCM label	JME scans		Independent samples	Cross-correlation between JME scans		Maxwellian histogram		
	Total	Reject		Mean	σ	Bins	χ_0^2 fit parameter	95% Threshold
1	9	0	335	5.7%	12%	16	12.3 42%ile	23.7
2	17	1[a]	336	5.6%	22%	13	11.5 65%ile	19.7

a. One JME scan was highly correlated with a previous scan.

Table 5 DCM DGD Results

DCM label	Length (km)	Mean DGD (ps)		$\frac{\sigma}{\mu}$	Conf. interval	PMD factor ps/$\sqrt{km}$	$\Delta\lambda_c$ (nm)	Correlation bandwidth constant ~1513
		Sample	Best fit					
1	7	1.48	1.50	41.9%	4.5%	0.567	3.70	5.5[a] - 0.72[b]
2	10	0.807	0.820	41.5%	4.5%	0.259	6.93	5.6 - 0.73

a. Units are nm ps.
b. Unit-less: Hz s.

The hypothesis of a Maxwellian fit is not rejected for either distribution.

Figure 6.5 DCM DGD Histograms

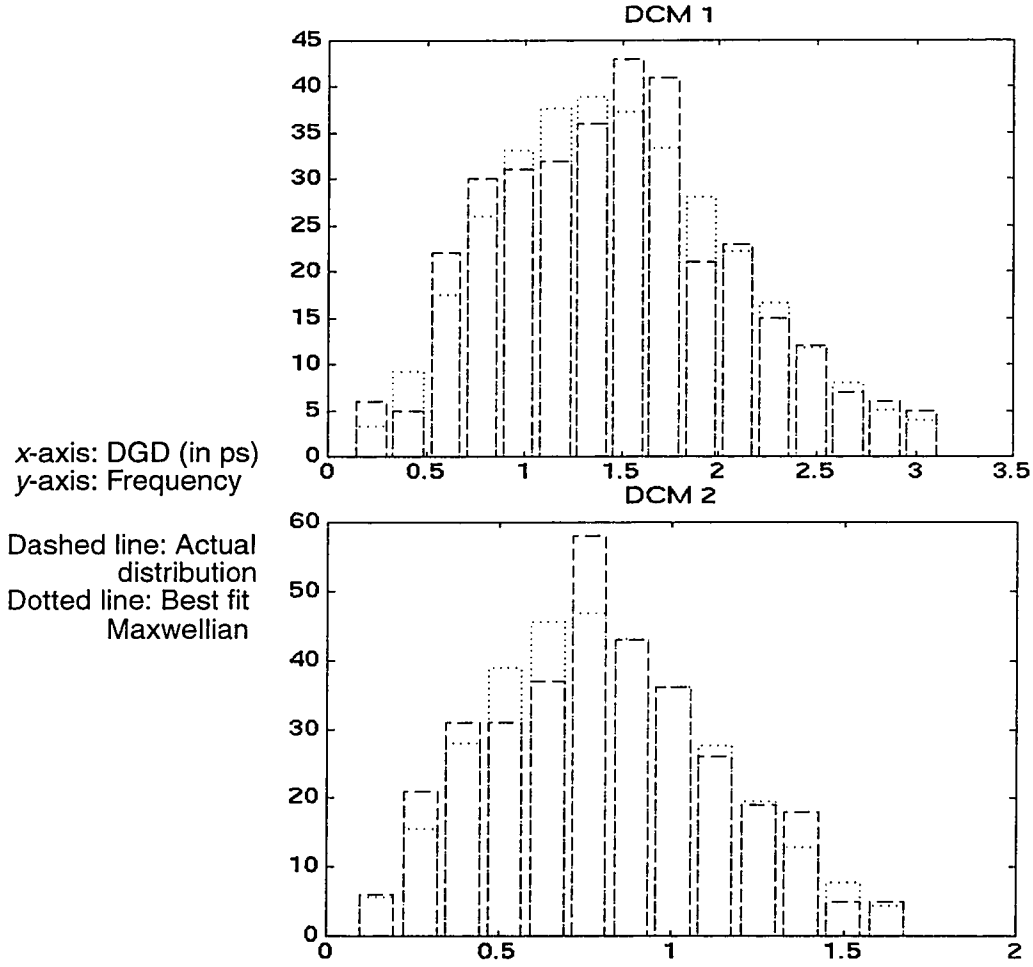

The DCMs both belong to the long-length PMD regime as exhibited by their close fit to a Maxwellian distribution. The average correlation bandwidth constant around 1513 nm was 5.6 nm.ps or 0.73 s.Hz, which is in close agreement to the predicted value.

6.3.4 EDFAs

JME scans of the Oprel fibre amplifier (EDFA-4) were taken at different temperatures within the range of -10 to 50 C, which is the operational temperature specified for the amplifier. The cross-correlation of the different JME scans remained above 50% over the temperature range, hence the correlation temperature could not directly be computed from the cross-correlation data. The correlation temperature was estimated by fitting a Gaussian envelope through the acquired correlation plot, and finding the full-width at half-maximum. The correlation temperature was estimated at approximately 100 C. Due to this high value, we conclude that the PMD instance of an EDFA cannot change if the EDFA is kept within its operational temperature range. For this reason, and since EDFAs in a typical communications setup are kept in controlled environmental conditions, these components were kept at constant temperature and treated as fixed DGD contributors in the experiment.

The EDFAs were measured before and after complete-system measurements to ensure their JME scan remained static. They were measured in 1 nm steps over the 1530 - 1560 nm range, at ambient laboratory temperature.

Due to the small number of samples and the fixed nature of the DGD in EDFAs used in this system, a goodness of fit test is not applicable. The standard deviation is calculated from all measured DGD values although they are not independent.

Table 6 EDFA DGD Results

EDFA label	JME scans	Number independent samples	Mean DGD (ps)	$\frac{\sigma}{\mu}$	Cross-correlation of JME scans over life-time
1 (Pirelli)	2	2	0.273	32.8%	99.4%
2 (Photonetics)	2	2	0.356	10.9%	99.5%
3 (AMOCO)	2	2	0.383	14.5%	90.6%
4 (Oprel)	2	2	0.301	12.0%	98.4%

The cross-correlation of the EDFA DGD characteristics over the life-time of the system is better than 90% in all cases, which supports the statement that the PMD of EDFAs remains constant in this experiment.

6.4 Cascaded Link Results

From preliminary estimates of the mean DGDs of the components, the expected mean DGD of the system is approximately:

$$\sqrt{\left(0.04\frac{\text{ps}}{\text{km}^{1/2}}\right)^2 \cdot 251\text{km} + 4(0.3\text{ps})^2 + 1.5\text{ps}^2 + 0.75\text{ps}^2} = 1.89\ \text{ps}. \quad (6.4.1)$$

Due to the presence of EDFAs in the system, the wavelength range of the JME is restricted to 1530-1560 nm. The correlation bandwidth is approximately 3.1 nm: a JME scan over the operational bandwidth provides approximately 10 independent DGD samples. For a 5% error on the estimation of the mean, with a significance level of 5%, 28 measurements of uncorrelated instances are required.

6.4.1 Complete Cascaded Fibre System

In standard practice, DCMs are kept with all other transmission equipment at constant environmental conditions. However, since the available DCMs were such a large contributor to the overall DGD, their instance was allowed to vary along with that of the fibre in the oven chamber. In Section 5.5, numerical simulations showed that keeping primary PMD contributors constant greatly correlates JME scans, by a mean correlation value of 40%, if using components with identical mean DGDs to those of the devices used in this experiment.

However, varying the instance of the DCMs with the fibre spools, and taking into consideration the conclusions of Section 6.3.1, the relation found between T_c and length would suggest that, for a nominal length of approximately 270 km, T_c would be 0.65 C. Nevertheless, measurements of the cascaded link were taken at least 10 C apart, ensuring that temperature excursions exceeded T_c to decorrelate the PMD instances.

The results of the cascaded link measurements are tabulated below:

Table 7 Cascaded Link Statistical Measurement Data

JME scans		Independent samples	Cross-correlation between JME scans		Maxwellian histogram		
Total	Reject		Mean	σ	Bins	χ_0^2 fit parameter	95% Threshold
32	6[a]+7[b]	209	8.8%	24%	12	3.622 3.7%ile	18.3

a. Not all measurements were taken at 23 C. Overall measurements still showed slight temperature dependence from 0 to 23 C (mean DGD increasing with temperature), and thus only ambient temperature measurements were kept.
b. Several JME scans were highly correlated with other scans.

Table 8 Cascaded Link DGD Results

Length (km)	Mean DGD (ps)		$\frac{\sigma}{\mu}$	Conf. interval	PMD factor $ps/\sqrt{km}$	$\Delta\lambda_c$ (nm)	Correlation bandwidth constant ~1545nm
	Sample	Best fit					
251.099	2.11	2.12	38.7	5.7%	0.133	2.57	5.4[a] - 0.68[b]

a. Units are nm ps.
b. Unit-less: Hz s.

The Maxwellian fit hypothesis was again not rejected, as the system exhibited the best fit of all DGD distributions acquired. It is noteworthy that the system's ratio of standard-deviation-to-mean DGD is further from the ideal value of 42.2% than any other component. The fact that the standard-deviation is smaller than the theoretical value may be due to the fixed character of the PMD in the EDFAs.

Figure 6.6 Cascaded Link DGD Histogram

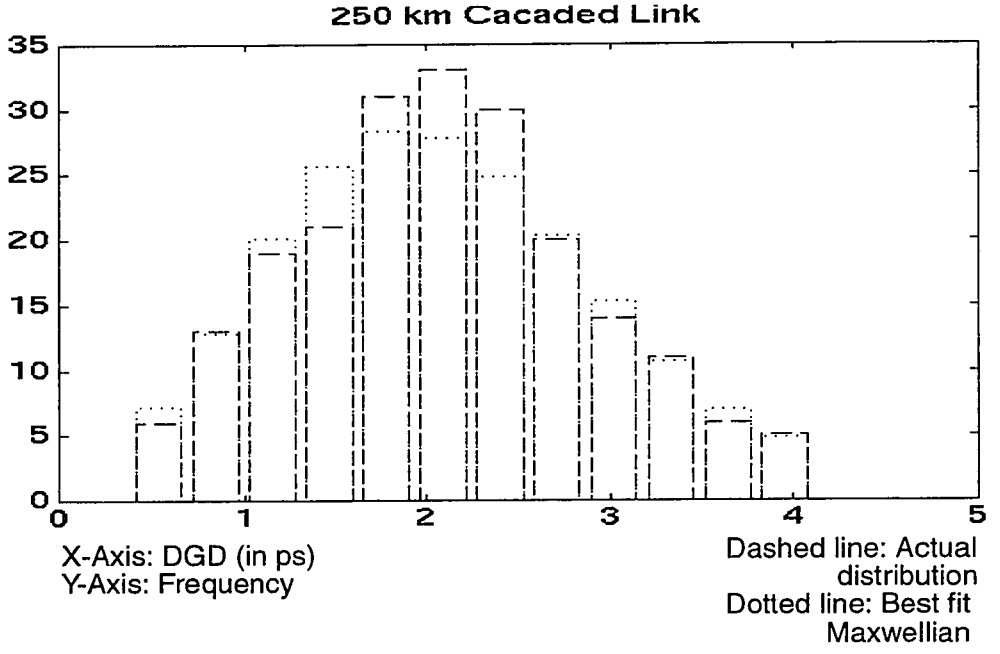

The correlation bandwidth $\Delta\lambda_c$ of the system is 2.77 nm in the vicinity of 1545 nm, for a correlation bandwidth constant of 5.4 nm.ps or 0.68 s.Hz, which is close to the expected value of 5.8 nm.ps or 0.75 s.Hz.

6.4.2 Cascaded Link Rule

The objective of the measurements in this experiment is to verify the cascaded link rule.

Table 9 System DGD Estimate Based on Components

Component	Sample Mean	Best Fit Mean	Standard Deviation	Confidence Interval
DCM 1	1.48	1.50	41.9%	4.5%[a]
EDFA 1	0.273		32.7%	7.9%[b]
Fibre 1	0.434	0.440	41.4%	4.7%
EDFA 2	0.356		10.8%	1.9%
Fibre 2	0.588	0.597	44.1%	4.7%
EDFA 3	0.383		14.5%	8.0%
Fibre 3	0.312	0.321	42.7%	6.5%
EDFA 4	0.301		12.0%	4.1%
DCM 2	0.807	0.820	41.5%	4.5%
Root Sum of Squares	1.98	2.00	0.792 40.0%	0.095 4.8%
Measured	2.11	2.12	0.82 38.7	0.12 5.7%

a. The confidence interval for varying PMD components (DCMs and Fibres) is evaluated as indicated in Section 4.7.
b. The confidence interval for fixed-PMD EDFAs is evaluated using the RMS of the difference between the start-of-life and end-of-life JME scan samples.

The confidence intervals of the measured and calculated values overlap, as shown in Figure 6.7:

Figure 6.7 Confidence Interval Overlap

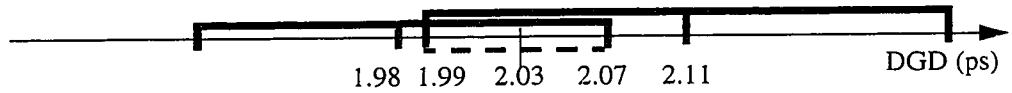

The overlap extends from 1.99 to 2.07 ps, which represents a 4.2% interval (+/-2.1%) around 2.03 ps, its median. These results are thus consistent with the cascaded link rule. Similarly, the values of calculated and measured standard deviation show close agreement. Despite the presence of fixed PMD components, these results agree with the PMD cascaded link rule.

6.5 Experimental Error

The experimental error between calculated and measured mean DGD is due to a combination of contributions, including measurement instruments, and optical effects.

The Poincaré representation on the HP 8509B polarimeter has an angular uncertainty of 1.5° (0.026 rad). From Section 4.1.2, this is equivalent to an uncertainty of 0.033 ps on the instantaneous DGD for 1 nm wavelength steps in the vicinity of 1545 nm. The uncertainty is inversely proportional to the wavelength step, and therefore increases by the same factor as the step decreases: for the smallest step used here (0.25 nm), the uncertainty increases to 0.133 ps. In this experiment, the wavelength step is chosen using an inversely proportional relation to the mean DGD (4.1.6). Therefore, the uncertainty due to polarimetry is approximately proportional to the mean DGD, with a relative uncertainty estimated at 4.4%.

The fixed PMD of EDFAs, representing 11% of the total (in root-sum-of-squares) can affect the total. Similarly, the cumulative effect of polarization dependent loss, which,

although negligible for these components, can also affect the accuracy of the measurements.

6.6 Result Summary

6.6.1 Component and System PMD Measurement Methodology

A new method of characterizing the PMD of optical communications equipment by varying temperature to create new statistical instances has been proven. Single mode fibre, Erbium doped fibre amplifiers, and dispersion compensating modules were characterized, as well as the communications system linking them. The cascaded link rule relating the PMD of a link to the PMD of the cascaded components was found to be true within experimental error.

This verification plan studied the cascaded link rule as it would apply in a typical optical communications setup, where some components have fixed DGD, while others vary. In a typical terrestrial system made of vintage fibre, the fibre would represent the highest DGD contribution, while the fixed elements (EDFAs, DCMs) would contribute residual DGD.

The cascaded link rule was measured using metrics of mean DGD and standard deviation of DGD. The measured mean DGD of the system was within the error bounds of the expected mean calculated from the mean DGD of the individual components. The standard deviations of all varying DGD components were within +/-4.5% of the 0.422 theoretical ratio of standard-deviation-to-mean DGD.

6.6.2 Goodness of Fit

For each component with varying PMD and for the cascaded link, the population of DGD samples were found to resemble a Maxwellian distribution by using the standard

goodness of fit test. All measured distributions easily passed the 5% significance threshold, as their χ_0^2 parameters were all in the 65 percentile of Maxwellian distributions.

6.6.3 Determination of Correlation Bandwidth Constant

The $\Delta\lambda_c$ and corresponding correlation bandwidth constant were evaluated for all varying DGD components. The constants were within 8.5% error of the expected value of 5.8 ps.nm or 0.75 s.Hz, which showed good agreement with simulations.

6.6.4 Determination of Correlation Temperature

T_c was successfully evaluated for several components of varying length. A dependence on length was found, which can (a) be extrapolated to correlation times t_c, and (b) be used to scale the correlation parameters (T_c, t_c) of a measured link to a subset of that link. For example, a looped back link having correlation time t_c is made up of two individual spans having correlation time t_c*sqrt(2).

6.6.5 Real-World Validity

Keeping environmental conditions constant, the mean DGDs averaged over JME scans were generally within the boundaries set by the real-world validity formula. Only one JME scan was rejected out of all the component and system measurements.

Chapter 7: Conclusion

7.1 Summary

The objective of the thesis was to validate the expression relating the PMD of cascaded links to the PMD of the link's constituents. Within experimental error, this goal was achieved, while the steps required for this task are outlined below.

The phenomenon called Polarization Mode Dispersion was described from a physical and a systems point of view. Its statistical properties were discussed including the Maxwellian probability density function which governs the distribution of differential group delay over time and wavelength. The effects of first and second-order PMD on a fibre optic communication link were discussed, and an expression for the penalty in terms of the mean DGD was given.

Three PMD measurement techniques were compared, namely the Jones matrix eigen-analysis, the wavelength scanning, and the interferometric methods. Due to availability and ease of statistical analysis, the JME method was selected for PMD measurements for this thesis. An expression for the variance in the estimate of the mean DGD (averaged over wavelength) was shown which relates the measurement bandwidth and the mean DGD itself to the expected variance.

The PMD numerical simulation program was described, and various results of its execution were commented upon. Empirical expressions were given for the variance in the mean DGD (averaged over wavelength), the error on limited bandwidth cross-correlation values, and the relation between the mean DGD and the PMD correlation bandwidth. The simulations conformed to a Maxwellian distribution using the χ_0^2 goodness of fit test.

Finally, to attain the goal of the thesis, a realistic confidence level for the outcome of the experimental measurements was specified. Based on this confidence level and the findings from the numerical simulations, an expression was derived to calculate the minimal number of measurements required, over wavelength and time. A cascaded link system was described, and its components were characterized in terms of PMD. The correlation bandwidth and temperature of the components were defined, and used to statistically explore their DGD characteristics. The measurements conformed to Maxwellian distributions where expected. The link itself was measured, and the mean DGDs of the link and its components were compared, with the main result that, within experimental and statistical error, the mean DGD of the whole was equal to the root sum of squares of the mean DGDs of its constituents.

7.2 Contribution

The contributions towards the study of PMD provided by this thesis are (a) an analysis of the amount of measurements required to close the confidence interval on the estimate of mean DGD, from a sample-counting perspective, (b) empirical determination by numerical simulation and measurement of the number of samples within a JME measurement (which also translates into measurement of the correlation bandwidth), and (c) generation of uncorrelated instances of PMD via determination of the correlation temperature. The relationship between fibre length and correlation temperature is an additional finding "picked up along the way". Finally, this thesis confirms that, with enough samples to limit the error on the mean, the population of DGD samples of a particular device adheres to a Maxwellian distribution.

The physical models and mathematics behind PMD are widely known and taken from the literature. The PMD measurement techniques described were developed by various parties and described in publications. Similarly, approximations of the variance of the estimate of the mean DGD (averaged over wavelength) are borrowed from references.

7.3 Suggestions for Further Work

Using the same order in which topics were discussed in this thesis, the following future work suggestions are made. From the modelling point of view, an analytical derivation of the correlation bandwidth would give confidence to the empirical result. Along with that, analytical derivations of the simulation results pertaining to variance on the mean and cross-correlation error would be desirable.

The measurements conducted in this thesis are laborious. For a long term PMD characterization test-bed, the processes of (a) determining the correlation temperature of a device and (b) generating independent PMD instances for a device and measuring the mean DGD should be automated, now that a methodology is in place. This would help narrow down the uncertainty on a device's mean DGD. In terms of statistical model characterization, automated measurements would permit a population of DGD samples large enough to characterize the tail of the distribution to be more easily obtained over a given period of time. This would help ascertain to a further degree the theoretical Maxwellian distribution.

It would appear that the possibilities of numerical simulations are endless. From this perspective, a pulse of given duration could be made to propagate through the fibre already created by the simulation program. After addition of this feature to the program, the pulse distorting effects could be examined, and consequential communications penalty

derived and compared to that of the literature. A study of PMD compensation could ensue from this.

Finally, given the limitations of the devices which were measured, and the knowledge that the major DGD contributors were devices which are usually passive, a test of a system with high PMD fibre spans would be ideal. In this case, the DCMs could be held at constant temperature, and only the PMD in fibre spools would have to vary over time (or temperature). Due to the high DGD, fewer measurements would have to be taken to obtain mean DGD estimates with the same confidence interval as obtained in this thesis. From the systems perspective, a link with high DGD could be used to further study the effects of first and second-order PMD over time.

References

[1] G.P. Agrawal, *Fiber-Optic Communications Systems*, New York: John Wiley & Sons, 1997.

[2] F. Bruyère, "Impact of First and Second-Order PMD in Optical Digital Transmission Systems," *Optical Fiber Technology*, pp. 269-280, January, 22, 1996.

[3] F. Bruyere and O. Audouin, "Assessment of system penalties induced by polarization mode dispersion in a 5 Gb/s optically amplified transoceanic link," *IEEE Photonics Technology Letters*, Vol. 6, pp. 443-445, January 1994.

[4] E. Collett, *Polarized Light: Fundamentals and Applications*, New York: Marcel Dekker Inc., 1993.

[5] F. Curti, B. Daino, Q. Mao, F. Matera, "Concatenation of polarisation dispersion in single-mode fibres," *IEE Electronics Letters*, Vol. 25, No. 4, p.290-92, February 1998.

[6] F. Curti, B. Daino ,G. De Marchis, F. Matera, "Statistical treatment of the evolution of the principal states of polarization in single-mode fibers," *Journal of Lightwave Technology*, Vol. 8, No. 8 , pp. 1162-66, August 1990.

[7] C. De Angelis, A. Galtarossa ,G. Gianello, et al., "Time evolution of polarization mode dispersion in long terrestrial links," *Journal of Lightwave Technology*, Vol. 10, No. 5, pp. 552-55, May 1992.

[8] M.O. van Deventer, G.J. Nagel, Huub, A. van Den, et al., "Improvement of polarisation mode dispersion tolerance in high bitrate systems," presented at European Conference on Optical Communications ECOC 93, pp. 473-476, 1993.

[9] G.J. Foschini and C.D. Poole, "Statistical theory of polarization dispersion in single mode fibers," *Journal of Lightwave Technology*, Vol. 9, No. 11, pp. 1439-1456, November 1991.

[10] A. Galtarossa, G. Gianello, C. Someda, et al., "In field comparison among polarization-mode-dispersion measurement techniques," *Journal of Lightwave Technology*, Vol. 14, No. 1, pp. 651-657, January 1996.

[11] N. Gisin, "Solutions of the dynamical equation for polarization dispersion," *Optics Communications*, Vol. 86, No. 5, pp. 371-373, December 1991.

[12] N. Gisin, B. Gisin, J.P. Von der Weid, et al. "How accurately can one measure a statistical quantity like polarization mode dispersion?," *IEEE Photonics Technology Letters*, Vol. 8, No. 12, pp. 1671-1673, December 1996.

[13] N. Gisin, J. P. Von der Weid, J. P. Pellaux, "Polarisation mode dispersion of short and long single-mode fibers," *Journal of Lightwave Technology*, Vol. 9, No. 7, pp. 821-827, July 1991.

[14] N. Gisin, R. Passy, P. Blasco, et al., "Definition of polarization mode dispersion and first results of the COST 241 round-robin measurement," *Pure Applied Optics*, Vol. 4, pp. 511-522, April 10, 1995.

[15] L.M. Gleeson, E.S.R. Sikora , M.J.O. Mahoney, "Experimental and numerical investigation into the penalties induced by second-order polarisation mode dispersion at 10Gb/s," presented at IEE European Conf. on Opt. Comm. IOOC-ECOC 97, Vol. 1, pp. 15-18, 1997.

[16] B.W. Hakki, "Polarization Mode Dispersion in a Single Mode Fibre," *Journal of Lightwave Technology*, Vol. 14, No. 10, pp. 2202-2208, October 1996.

[17] B.L. Heffner, "Automated measurement of polarization mode dispersion using Jones matrix eigenanalysis," *IEEE Photonics Technology Letters*, Vol. 4, No. 9, pp. 1006-1009, September 1997.

[18] B.L. Heffner, "Compensation formula for noise threshold bias of interferometric PMD measurement," in NIST Technical Digest: Symposium on Optical Fiber Measurements 1996, Vol. 905, pp. 135-138, 1996.

[19] P. Kaminow, "Polarization in optical fibers," *IEEE Journal of Quantum Electronics*, Vol. QE-17, pp. 15-22, January 1981.

[20] E. Kreyszig, *Advanced Engineering Mathematics*, 7th Ed., Toronto: John Wiley & Sons Inc, 1993.

[21] A.V. Oppenheim, R.W. Schafer, *Discrete-Time Signal Processing*, New Jersey: Prentice Hall, 1989.

[22] C.D. Poole, R.W. Tkach, A.R. Chraplyvy, et al., "Fading in lightwave systems due to polarization-mode dispersion," *IEEE Photonics Technology Letters*, Vol. 3, pp. 68-70, January 1991.

[23] C.D. Poole, D.L. Favin, "Polarization Mode Dispersion Measurements Based on Transmission Spectra Through a Polarizer," *Journal of Lightwave Technology*, Vol. 12, No. 6, pp. 917-929, June 1994.

[24] C.D. Poole, J.H. Winters, J.A. Nagel, "Dynamical equation for polarization dispersion," Optics Letters, Vol. 16, No. 6, pp. 372-374, March 1991.

[25] C.D. Poole and R.E. Wagner, "Phenomenological approach to polarization dispersion in long single-mode fibres," *IEE Electronics Letters*, Vol. 22 , No. 19, pp. 1029-1030, September 11 1986.

[26] C.D. Poole, "Statistical Treatment of Polarization Dispersion in Single-Mode Fiber," *Optics Letters*, Vol. 13, No. 8, pp. 687-689, August 1988.

[27] C.D. Poole, N. S. Bergano, R.E. Wagner, et al., "Polarization Dispersion and Principal States in a 147-km Undersea Lightwave Cable," *IEEE Journal of Lightwave Technology*, Vol. 6, No. 7, pp. 1185-1190, July 1988.

[28] Product Documentation, *Polarization Mode Dispersion by the Jones Matrix Eigenanalysis and Wavelength-Scanning Methods*, Santa Rosa: Hewlett-Packard Company, Lightwave Operation, 1995.

[29] S.C. Rashleigh and R. Ulrich, "Polarization mode dispersion in single-mode fibers," *Optics Letters*, Vol. 3, No. 3, pp. 60-62, August 1978.

[30] B.E.A. Saleh, M.C. Teich, *Fundamentals of Photonics*, USA: John Wiley & Sons, 1991.

[31] D. Watley, "PMD Stationarity," NORTEL Proprietary Paper, Sep 1997.

[32] P.A. Williams, "TIA round robin for the measurement of PMD," in NIST Technical Digest: Symposium on Optical Fiber Measurements 1996, Vol. 905, pp. 155-158, 1996.

IMAGE EVALUATION
TEST TARGET (QA-3)

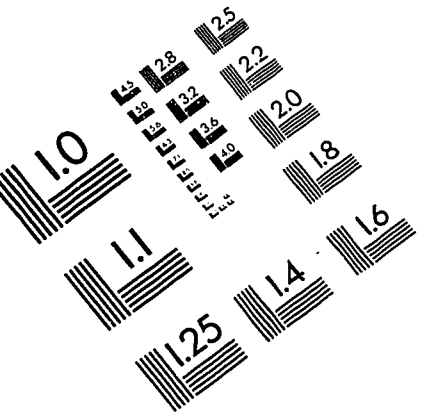

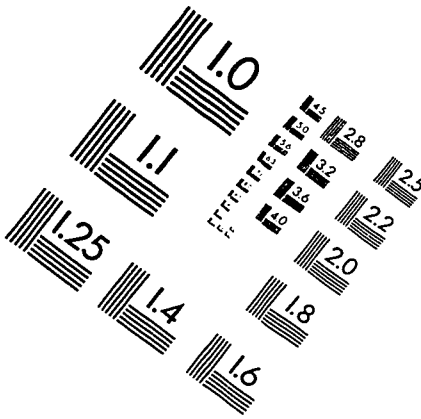

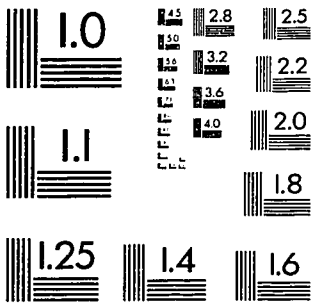

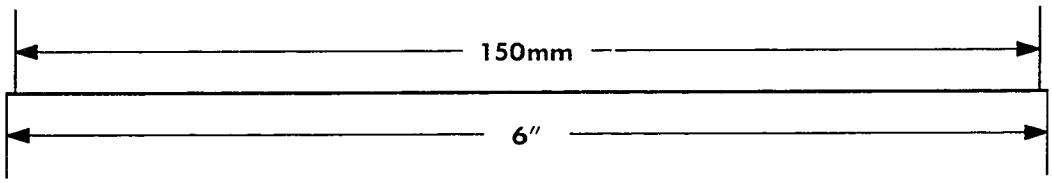

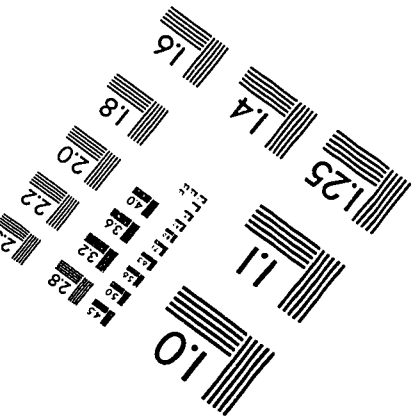

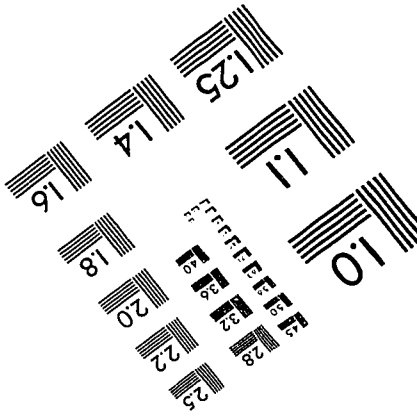

APPLIED IMAGE, Inc
1653 East Main Street
Rochester, NY 14609 USA
Phone: 716/482-0300
Fax: 716/288-5989